Triassic and Jurassic radiolarian response to global catastrophic events in the Panthalassa Ocean, as recorded in the Mino Belt, central Japan

Tetsuji ONOUE*, Rie S. HORI** and Satoru KOJIMA***

Abstract

The field trip will focus on the radiolarian response to global catastrophic events (e.g., bolide impact, large-scale volcanism, and anoxia) recorded in Triassic and Jurassic radiolarian chert of the Mino Belt, central Japan. The radiolarian chert of the Mino Belt records the sedimentary history of an oceanic plate in the Panthalassa Ocean prior to accretion at the trench. The topics presented and discussed in the field are: (1) the end-Permian mass extinction and recovery from the event; (2) Early Triassic anoxia and subsequent recovery in the Middle Triassic; (3) paleoenvironmental changes across the Early–Late Carnian boundary (Carnian Pluvial Event); (4) collapse of marine ecosystems triggered by a Norian impact event; (5) ocean acidification at the Triassic–Jurassic boundary; and (6) Early Jurassic (Toarcian) anoxia and the formation of black chert. In addition to these topics, this trip will consider aspects of the accretion process of oceanic plate sediments during the Middle to Late Jurassic.

Key words: Triassic, Jurassic, Radiolaria, chert, Mino Belt, accretionary complex

* Department of Earth and Environmental Sciences, Faculty of Advanced Science and Technology, Kumamoto University, Kumamoto 860-8555, Japan

** Department of Earth Sciences, Graduate School of Science and Engineering, Ehime University, Matsuyama 790–8577, Japan

*** Department of Civil Engineering, Faculty of Engineering, Gifu University, Gifu 501–1193, Japan
Corresponding author: T. Onoue,
onoue@sci.kumamoto-u.ac.jp

(Manuscript received 18 June, 2017; accepted 24 July, 2017)

Introduction

The aim of this field trip is to introduce the stratigraphy and micropaleontology of sections through Lower Triassic–Middle Jurassic sequences of the Mino Belt in central Japan. The Mino Belt is a Middle to Late Jurassic subduction-generated accretionary complex in central Japan that strikes approximately east-northeast (Fig. 1). The belt is characterized by a coherent sequence comprising Lower Triassic to Middle Jurassic bedded chert and overlying Middle Jurassic terrigenous clastic rocks (Matsuda and Isozaki, 1991). The absence of carbonate rocks and coarse terrigenous grains in the bedded chert suggests that its primary depositional site was deeper than the calcium carbonate compensation depth and beyond the reach of terrigenous clastic grains. Previous paleomagnetic studies of the Triassic bedded chert successions of the Mino Belt suggested that these sediments accumulated in a pelagic, open-ocean setting within a low- to middle-latitude part of the Panthalassa Ocean (Shibuya and Sasajima, 1986; Ando et al., 2001; Uno et al., 2015). The Triassic–Jurassic cherts accreted within an accretionary complex on the eastern margin of the Asian continent during the Middle to Late Jurassic (Matsuda and Isozaki, 1991).

The Triassic–Jurassic chert sequences of the Mino Belt in the Inuyama–Kamiaso area, central Japan, preserve one of the most significant and complete records of Triassic–Jurassic pelagic environments in the Panthalassa Ocean. The three-day field trip will focus on the radiolarian response to global catastrophic events (e.g., bolide impact, large-scale volcanism, and anoxia) recorded in the Triassic to Jurassic radiolarian chert in the Inuyama–Kamiaso area. Equally importantly, we hope to provide the participants with knowledge of aspects of the accretion process of oceanic plate sediments during the Middle to Late Jurassic.

Geologic outline of the Inuyama–Kamiaso area

1. General overview

The Mino Belt consists of Jurassic accretionary complexes that strike east–northeast in central Japan (Fig. 1). The belt is juxtaposed against the Circum–Hida (Hida Gaien) Belt to the north, which is tectonically overlain by the metamorphosed correlative of the Mino Belt that occurs to the south (the Ryoke Belt).

The accretionary complexes in the Mino Belt are subdivided into seven tectonostratigraphic units based on lithology, structure, and age of accretion (Fig. 2: Wakita, 1988; Wakita et al., 1992). The complexes consist of two coherent units (the Samondake and Kamiaso units) and five melange units (the Sakamoto-toge, Funafuseyama, Kuze, Nabi, and Kanayama units). The coherent units are composed of imbricate thrust sheets of sedimentary sequences that retain their primary stratigraphic coherency in most parts. The

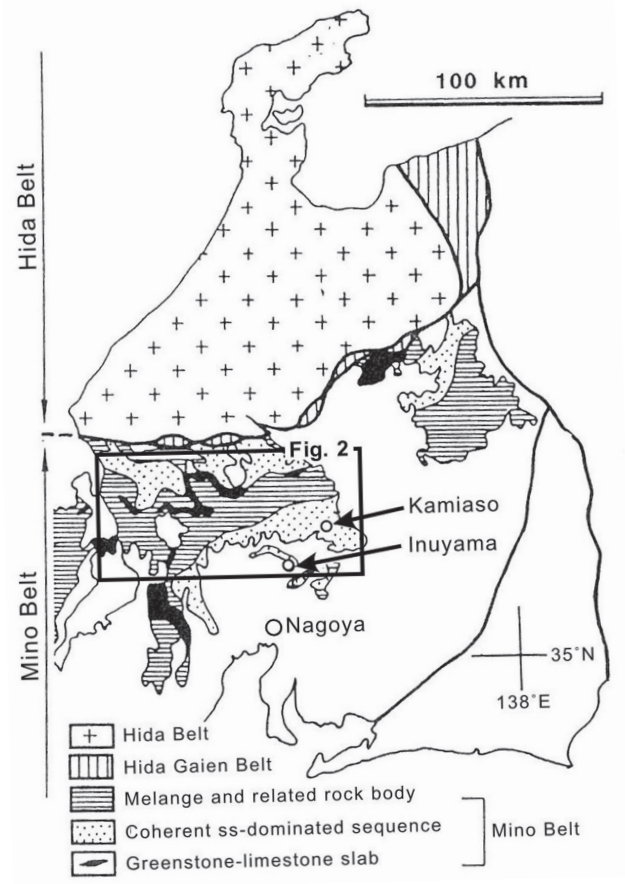

Fig. 1. Index map showing the Inuyama–Kamiaso area (modified from Matsuoka et al., 1994).

melange units consist of mixed rock assemblages in which numerous blocks and lenses of various lithologies (e.g., basaltic rocks, limestone, and bedded chert) and size are complexly mingled with terrigenous clastic rocks (Wakita, 1988; Nakae, 2000; Sano and Kojima, 2000; Sano et al., 2017). The ages of accretion of these units become younger from north to south, as the structurally lower units occur in the southern area (Wakita, 1988; Wakita et al., 1992).

The field trip will visit seven localities in the Inuyama–Kamiaso area, eastern Gifu Prefecture, central Japan (Figs. 2, 3). This area is distributed in the southern part of the coherent Kamiaso Unit of the Mino Belt, which strikes east–northeast. The Kamiaso Unit in this area consists of thrust piles of sedimentary sequences containing Triassic to Lower Jurassic bedded chert and overlying Middle Jurassic clastic rocks (i.e., a chert–clastic sequence: Matsuoka et al., 1994). The chert–clastic sequence is interpreted to have accumulated in a pelagic, deep-sea setting below the carbonate compensation depth and within a tapering wedge of trench-fill turbidites with distal facies. Paleomagnetic analysis of the bedded chert in the study area indicates that the site of deposition changed from a low-latitude zone in the Middle Triassic to a mid-latitude zone in the Late Triassic (Fig. 4:

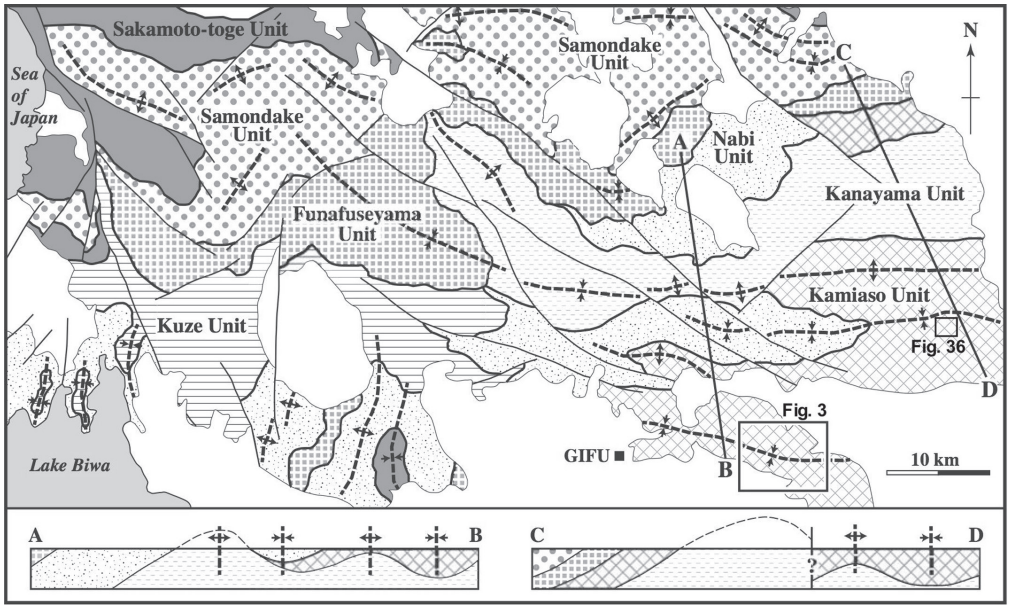

Fig. 2. Map showing the tectonostratigraphic subdivision of the accretionary complexes in the Mino area and geological cross-sections along the lines A–B and C–D. After Kojima et al. (2016).

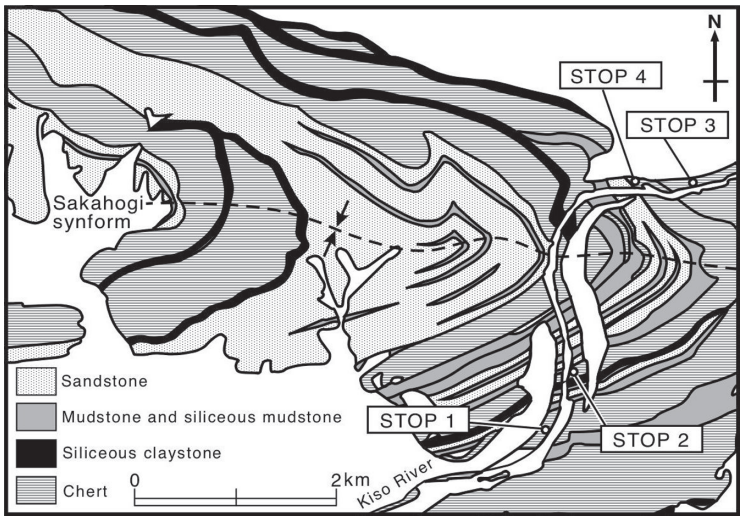

Fig. 3. Geologic and location maps of the field stops along the Kiso River. Modified after Wakita (1988).

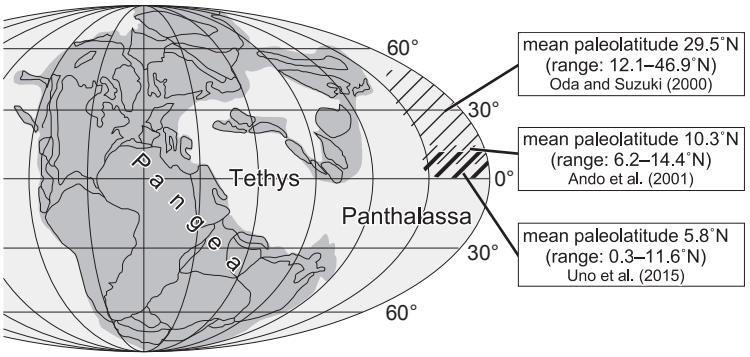

Fig. 4. Late Triassic paleogeography showing the paleolatitudes for the site of deposition of the Inuyama chert (after Uno et al., 2015). The data for the Inuyama chert is of Norian age.

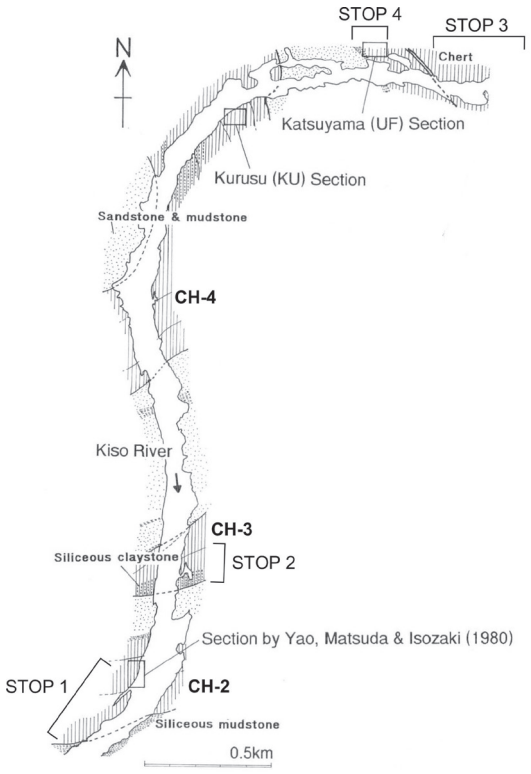

Fig. 5. Route map of the chert-clastic sequence along the Kiso River in the Inuyama area. Modified after Hori (1992).

Shibuya and Sasajima, 1986; Oda and Suzuki, 2000; Ando et al., 2001; Uno et al., 2015). Previous studies have compiled a detailed radiolarian biostratigraphy of the Triassic to Middle Jurassic bedded chert of the area (e.g., Yao et al., 1982; Hori, 1990, 1992; Sugiyama, 1992, 1997).

The chert–clastic sequence in the Inuyama–Kamiaso area occurs as a stack of thrust sheets (Wakita, 1988; Kimura and Hori, 1993) that formed during accretion (Matsuda and Isozaki, 1991) and are named CH-1, CH-2, CH-3, and CH-4, in structurally ascending order (Yao et al., 1980). The complexly stacked wedges of the thrust sheets form a large syncline (the Sakahogi Synform) that plunges to the west (Fig. 5).

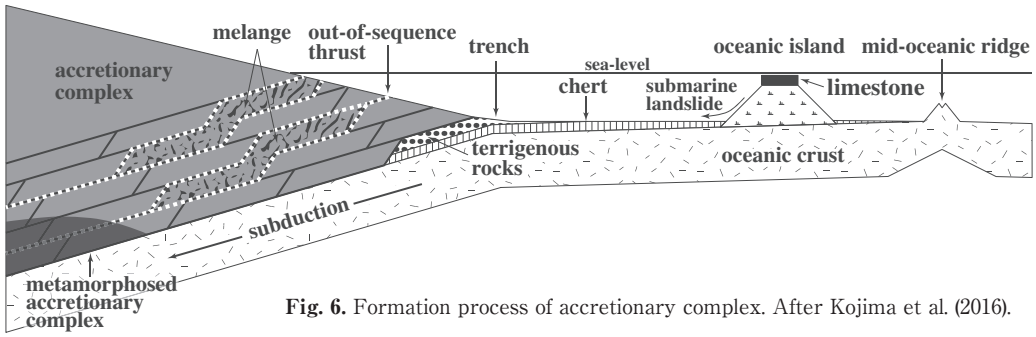

Fig. 6. Formation process of accretionary complex. After Kojima et al. (2016).

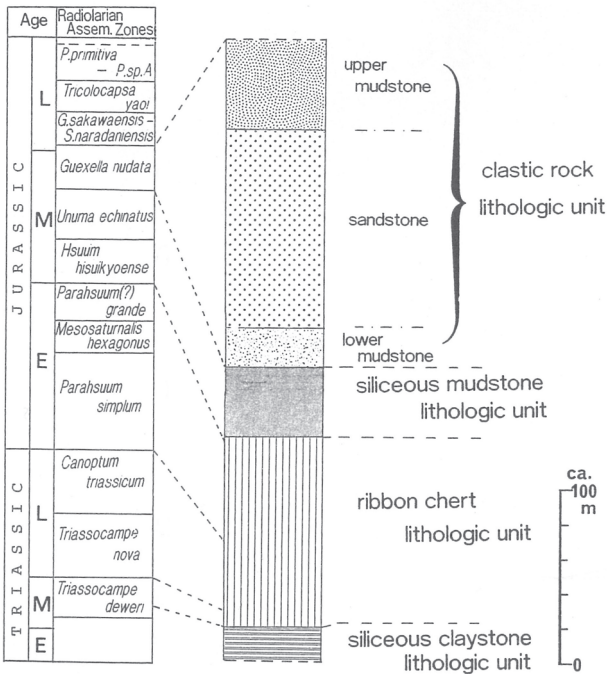

Fig. 7. Generalized columnar section of Triassic–Jurassic chert–clastic sequence in the Inuyama area (modified after Kimura and Hori, 1993). Radiolarian assemblage zones are after Yao et al. (1980) and Hori (1990).

2. Deep-water oceanic plate stratigraphy

The chert–clastic sequence records the sedimentary history upon an oceanic plate prior to accretion at the trench (Matsuda and Isozaki, 1991). The reconstructed ocean floor sequence found in ancient accretionary complexes is called "oceanic plate stratigraphy" and records the history of the oceanic plate from its initiation at a mid-ocean ridge to a trench where accretionary complexes are formed through offscraping and underplating of the oceanic plate (Fig. 6).

The chert–clastic sequence in the Inuyama–Kamiaso area is lithostratigraphically subdivided into lower siliceous claystone (ca. 19 m thick), middle bedded chert (ca. 110 m), upper siliceous mudstone (ca. 38 m), and uppermost clastic rocks (ca. 190 m) units in ascending order (Fig. 7: Kimura and Hori, 1993; Matsuoka et al., 1994). The stratigraphic

base and top of the sequence are truncated by thrust faults (Kimura and Hori, 1993). Studies of radiolarian and conodont biostratigraphy (e.g., Yao et al., 1982; Hori, 1990; Matsuda and Isozaki, 1991; Sugiyama, 1997) have revealed that the lower, middle, upper, and uppermost units of the chert–clastic sequence can be assigned to the upper Spathian to lower Anisian, middle Anisian to upper Toarcian, upper Toarcian to Bathonian, and Bathonian to lower Callovian, respectively.

The lower to upper units of the chert–clastic sequence record a Lower Triassic to Middle Jurassic sequence (~80 Myr). The lithostratigraphic change within the uppermost unit of the chert–clastic sequence indicates a lateral shift of the depositional sites as the oceanic plate migrated, from a pelagic setting during the deposition of the Lower Triassic to Lower Jurassic bedded chert to a hemipelagic setting, in which airborne tephras and fine-grained terrestrial materials were deposited, during Middle Jurassic time (Matsuda and Isozaki, 1991). The age of accretion of the chert–clastic sequence is best approximated as Middle Jurassic, as inferred from the youngest age of radiolarians obtained from black mudstone.

3. Triassic and Jurassic radiolarian biostratigraphy

Bedded cherts in the Mino Belt commonly yield Triassic–Jurassic radiolarians and Triassic conodonts. The depositional ages of the chert–clastic sequence in the Kamiaso Unit were initially dated using conodonts in the late 1970s and early 1980s (Igo and Koike, 1975; Koike, 1979; Isozaki and Matsuda, 1982, 1983; Yao et al., 1982). However, conodonts are so scarce in these cherts that the ages of the deposits were predominantly determined from the radiolarian biostratigraphy. Because the Triassic–Jurassic bedded chert successions in the Inuyama–Kamiaso area represent one of the most complete and well-preserved stratigraphic records in the Mino Belt, many radiolarian biostratigraphies have been established for the Triassic and Jurassic bedded cherts in this area (e.g., Nakaseko and Nishimura, 1979; Yao et al., 1980, 1982; Yao, 1982; Kido et al., 1982; Mizutani and Kido, 1983; Yoshida, 1986; Hori, 1990, 1992, 1997; Matsuda and Isozaki, 1991; Sugiyama, 1992, 1997).

In a landmark study of Triassic radiolarian biozones, Sugiyama (1997) established 18 radiolarian zones ranging from the Spathian (late Olenekian) to the end of the Triassic in siliceous rocks (chert and siliceous claystone) in the Inuyama–Kamiaso area of central Japan (Fig. 8). Sugiyama (1997) determined the total ranges of 247 selected radiolarian taxa based on high-resolution analyses of 534 samples from 26 sections along the Kiso and Hida rivers. He correlated these ranges with nine previously reported biozones worldwide and then determined the chronology of the radiolarian zones by compiling existing age data. This is the most comprehensive study on the subject to date, and the zonation scheme reported is the only one to span almost the whole Triassic with relatively high resolution (O'Dogherty et al., 2010). To calibrate Sugiyama's Triassic radiolarian zonation with the conodont zones

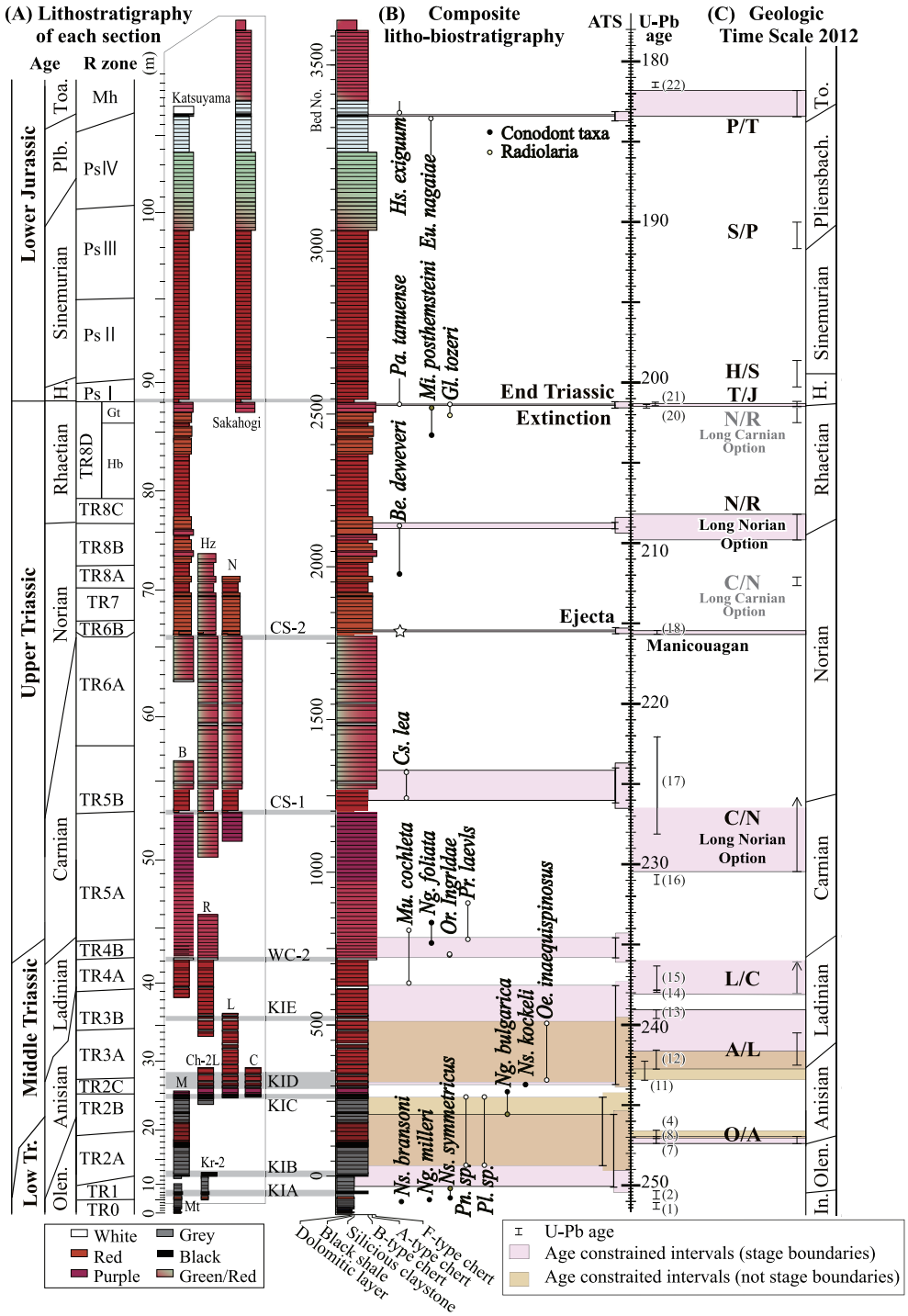

Fig. 8. The lithostratigraphy of the study sections and the composite litho-biostratigraphy for the Lower Triassic to Lower Jurassic deep-sea sequence in the Inuyama area, Japan. Lithologic types are from Sugiyama (1997), Ikeda et al. (2010) and Sakuma et al. (2012). After Ikeda and Tada (2014).

and the standard Triassic timescale, the Late Triassic conodont biostratigraphy was recently investigated in the same sections as those used by Sugiyama (1997) as type sections for radiolarian biozones (Nakada et al., 2014; Uno et al., 2015).

The first comprehensive work on the biostratigraphy of Jurassic radiolarians in the Inuyama–Kamiaso area was carried out by Yao et al. (1980). Subsequently, Yao (1982) described three Triassic and one Jurassic radiolarian assemblages in the CH-2 thrust sheet along the Kiso River in the Inuyama area. As a result of extensive research on Lower and Middle Jurassic bedded cherts, Hori (1990) established five radiolarian assemblage-zones in this area. In chronological order, these are the *Parahsuum simplum* I, *P. simplum* II, *P. simplum* III, *P. simplum* IV, *Mesosaturnalis hexagonus*, *Parahsuum* (?) *grande*, and *Hsuum hisuikyoense* zones (Fig. 8). The calibration for the Jurassic radiolarian zonation proposed by Hori (1990) with the standard Jurassic timescale is based on indirect correlation with ages determined from European and North American radiolarian biostratigraphies (Carter and Hori, 2005; Carter et al., 2010).

Stop descriptions

Figure 9 shows the localities visited during this field trip. Figures 3 and 5 presents a geological map of the Inuyama area showing the locations of Stops 1 to 4.

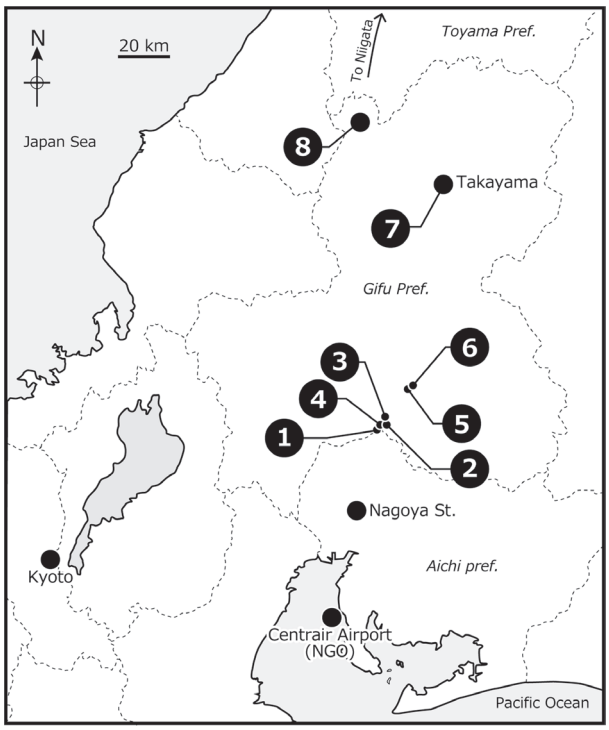

Fig. 9. Index map showing the field stops.

STOP 1. Unuma

GPS coordinates: 35° 23'54"N, 136° 57'33"E.

Unuma is well-known type locality of the genus *Unuma* described by Ichikawa and Yao (1976). The section at the Unuma locality consists of a ~60-m-thick sequence of bedded cherts of the CH-2 thrust sheet described by Yao et al. (1980). This is the renowned section where Yao et al. (1982) first established the four Middle Triassic to Lower Jurassic radiolarian zones in Japan. After their work, many studies of stratigraphy (Matsuda and Isozaki, 1991; Ikeda et al., 2010), structural geology (Kimura and Hori, 1993; Kameda et al., 2012), geochemistry (Takiguchi et al., 2006; Yamaguchi et al., 2016), and paleomagnetism (Shibuya and Sasajima, 1986; Ando et al., 2001) have been carried out at Unuma.

Stop 1-1: Recovery from superanoxia

The section at Unuma begins with carbonaceous claystone and black chert at the base (Ujiie et al., 2015), but the exposure of these rocks is now covered by gravel and sand.

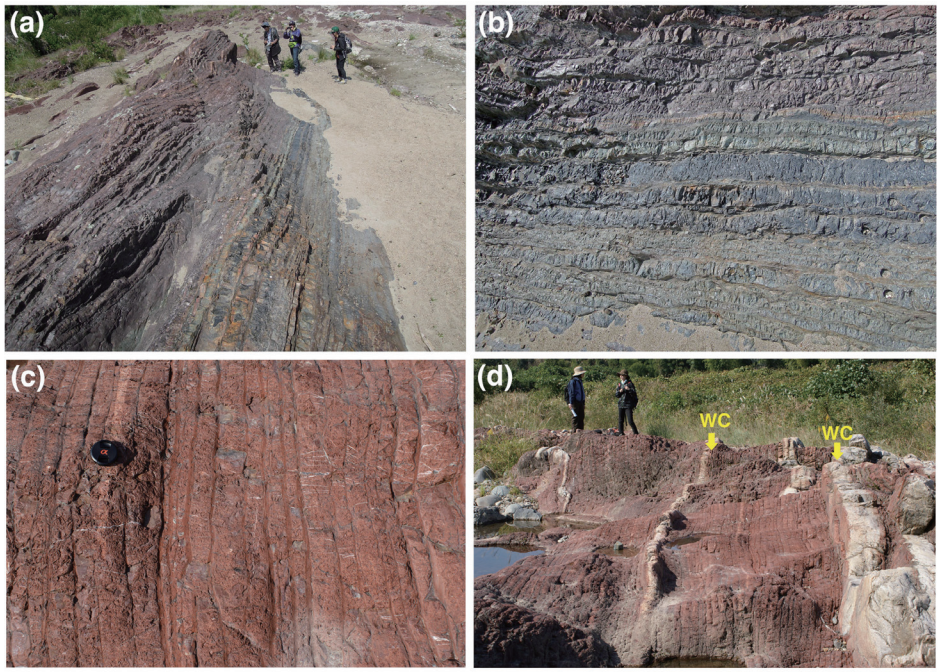

Fig. 10. Field occurrence of Middle Triassic bedded chert in the Unuma section. **(a)** Lower Middle Triassic (Anisian) bedded chert showing a remarkable redox change in deep-sea sediment; recovery from the dark gray anoxic chert to reddish oxic chert. **(b)** Sedimentary transition between gray to purple/brick red chert, reflecting an upward increase in hematite content. **(c)** Bedded chert consists of rhythmic alternations of chert and shale beds, which is considered to have resulted from cyclic changes in the accumulation rate of biogenic SiO_2 within a background of slow accumulation of eolian clay. **(d)** Rhythmic white chert (WC) layers interbedded with red cherts.

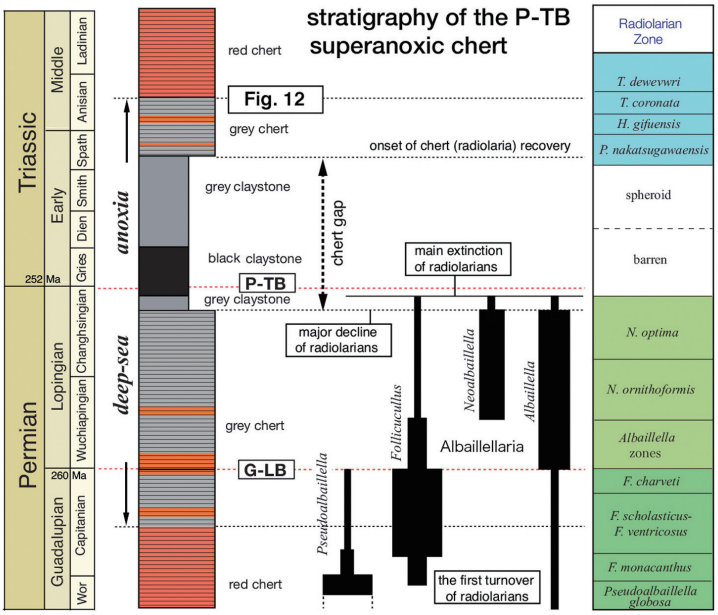

Fig. 11. Composite stratigraphic column of the Permian–Triassic boundary section in pelagic chert facies of Panthalassa (after Isozaki, 2014).

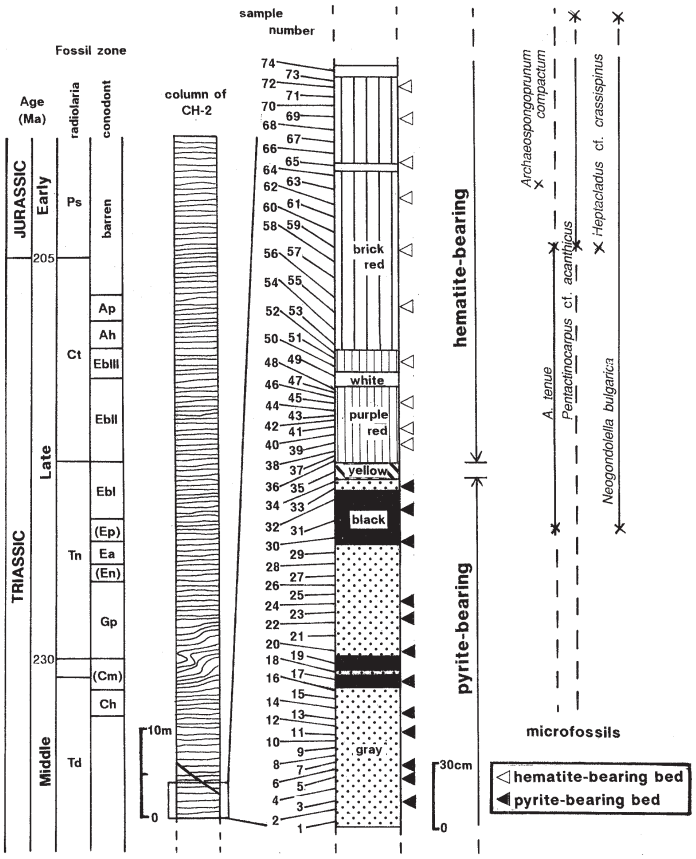

Fig. 12. Stratigraphic column of the study section showing distribution of hematite and pyrite (after Nakao and Isozaki, 1994).

Where depositional contacts occur, middle Anisian gray bedded chert overlies black chert. The gray bedded chert in the lowermost part gradually changes upward to red bedded chert (Fig. 10a, b), which represents the middle Triassic recovery from the deep-sea anoxic event that occurred across the Permian–Triassic boundary (Fig. 11: Isozaki, 1997). Based on Fe-mineral identification by Mössbauer spectroscopy, accessory Fe-bearing minerals in deep-sea cherts, such as pyrite and hematite, have been used as redox indicators for ancient deep-sea environments (Sato et al., 2011, 2012). Kubo et al. (1996) revealed that the occurrence of pyrite and hematite in the gray and red cherts essentially indicates primary reducing and oxidizing depositional conditions, respectively (Fig. 12). It is important to note that the oxygen-depleted interval was not restricted to the Permian–Triassic boundary, but had a much longer duration, until the middle Anisian (~10 Myr of the Triassic).

Stop 1-2: Milankovitch cycles

Middle Triassic red bedded cherts are continuously exposed along the Kiso River (Fig. 10c). The chert consists of rhythmically alternating beds of chert (5–135 mm in thickness) and thin beds of shale (1–80 mm thick). The processes that result in chert–shale couplets of alternating SiO_2-rich (chert) and SiO_2-poor (shale) beds have long been discussed. Hori et al. (1993) proposed that the chert beds were produced by radiolarian blooms against a background of constant, extremely slow accumulation of clay, based on the 10–100 times higher abundance of cosmic microspherules in shale than in chert (Fig. 13). They also

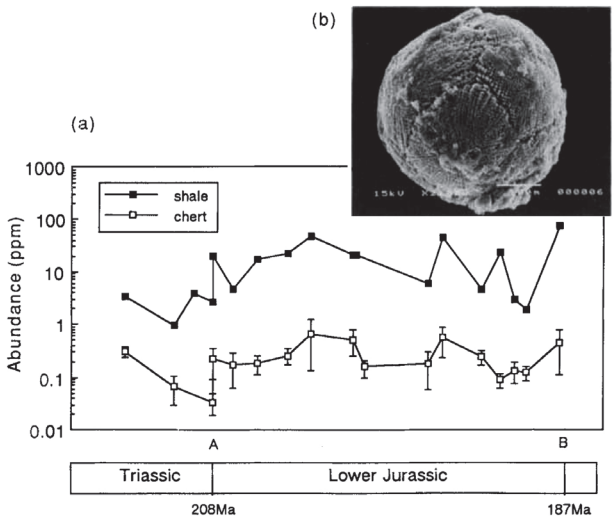

Fig. 13. The temporary change of magnetic microspherule abundance from shale and chert beds in the bedded cherts of the KU Section. Abundance is shown in ppm of volume from a pair of shale–chert couplet. The abundance value of cherts indicates the average of five samples. (b) Scanning electron micrograph of a representative magnetic microspherule which was obtained from the measured section. It has a characteristic dendritic form surface. Scale bar = 100 μm. After Hori et al. (1993).

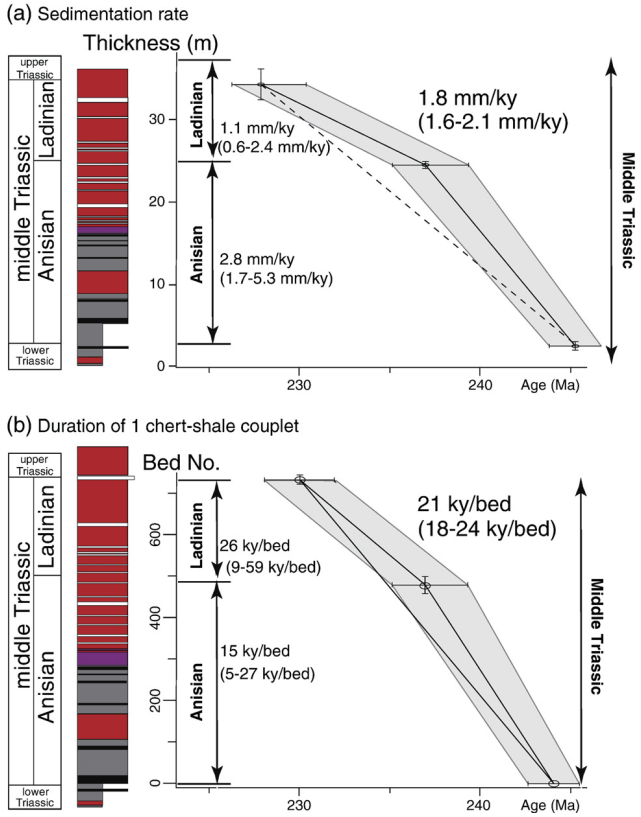

Fig. 14. (a) The estimated average sedimentation rates based on the relationship between thickness and age. **(b)** The estimated average duration of individual chert–shale couplets based on the relationship between bed number and age for the Anisian, Ladinian, and entire middle Triassic bedded chert in the Inuyama area, Central Japan. After Ikeda et al. (2010).

suggested that the bed-thickness cycles recognized in the bedded cherts were formed by periodic variations in radiolarian productivity related to the Milankovitch climatic cycle. Recently, spectral analysis of a bed-number series of thickness variations in chert beds was performed assuming that each chert–shale couplet represents a 20-kyr precession cycle in the Middle Triassic (Fig. 14: Ikeda et al., 2010). The results of spectral analysis revealed cycles involving approximately 200, 20, 5, and 2–3 beds, corresponding to periodicities of approximately 4000, 400, 100, and 40–60 kyr, respectively. By further assuming that the 20-bed cycle represents a 405-kyr eccentricity cycle of constant and stable periodicity, spectral analysis of the time series of thickness variations of chert beds revealed distinct 38-kyr obliquity and 97- and 117-kyr eccentricity cycles in addition to a 405-kyr eccentricity cycle (Ikeda et al., 2010). Although radiolarian productivity probably affected variations in chert bed thickness, further studies are required to understand the relationship between Milankovitch cycles and radiolarian productivity in the Triassic pelagic realm.

Stop 1-3: Origin of white chert

Rhythmically repeated white chert layers (~20 cm thick) are visible in the Anisian red bedded cherts at Unuma (Fig. 10d). The white chert is characterized by outcrop-scale

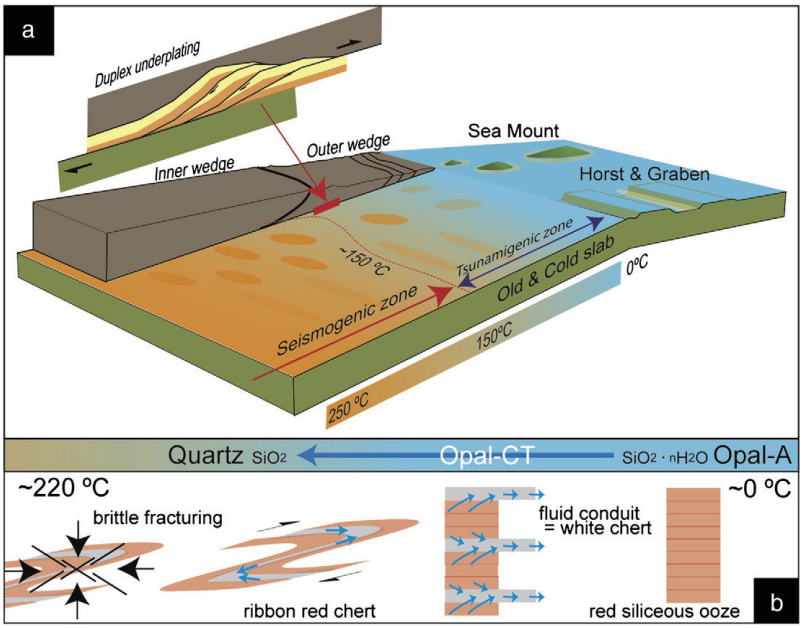

Fig. 15. Cartoon showing the setting of deformation/diagenesis of bedded cherts in a cold subduction zone (after Kameda et al., 2012). **(a)** Thermal conditions of a cold subduction zone. The temperature around seamounts (petit hot spot) and horst–grabens may be higher than that of normal oceanic plate due to volcanism, thereby representing hot patches in the subduction zone (future coupling areas). **(b)** Diagenesis of siliceous ooze (opal-A), resulting in its conversion to chert (i.e., quartz via an intermediate stage of opal-CT) accompanied by dehydration. White cherts represent fossilized fluid conduits during diagenesis. Brittle fracturing of the chert occurred after duplex-underplating under temperatures of ~220 °C.

ductile folding with ENE–WSW trending axial traces, and is composed mainly of thin crack-filling mineral veins that were precipitated in multiple stages. Kameda et al. (2012) suggested that the ductile deformation was facilitated by silica dehydration–precipitation, and is represented by multiple phases of vein networks.

The outcrop clearly shows that the white chert was formed prior to the ductile deformation. There are several hypotheses regarding the origin of the white cherts. Tsukamoto (1989) proposed that they were derived originally from limestones and were subsequently silicified during later burial diagenesis. In contrast, Kameda et al. (2012) suggested that the white cherts acted as conduits for SiO_2-oversaturated fluid and became silicified through multiple veining events and the precipitation of SiO_2 minerals, due to intense brittle fracturing and fluid flow (Fig. 15). Yamaguchi et al. (2016) estimated that the amount of water necessary to precipitate SiO_2 in the white chert is ~10^2 times larger than that produced from compaction and silica/clay diagenesis of pelagic siliceous sediment (chert). They pointed out that water released by dehydration during silica diagenesis and fluid from various other sources (e.g., smectite–illite transition, saponite–chlorite transition, and serpentine dehydration) would pass through the chert layer.

STOP 2. Momotaro Shrine

GPS coordinates: 35° 24'16"N, 136° 57'48"E.

The outcrop at STOP 2 is located near the Momotaro Shrine (Jinja) on the east side of the Kiso River in Inuyama City (Fig. 5). A widespread exposure of the Lower Triassic siliceous claystone and overlying Middle Triassic chert in the chert–clastic sequence of the CH-3 thrust sheet is visible (Fig. 16). Higher in the section, the Middle to Upper Triassic (Ladinian to Carnian) bedded chert is exposed.

Stop 2-1: Early Triassic anoxia

The Early to Middle Triassic radiolarian biostratigraphy at Momotaro Shrine was documented by Yao and Kuwahara (1997). This section was called the "Momotaro–Jinja section" (Fig. 17: Yao and Kuwahara, 1997). Three radiolarian biozones are recognized in the Lower Triassic siliceous claystone of this section: the Olenekian "Sphaeroides" and *Parentactinia nakatsugawaensis* zones, and the Anisian *Hozmadia gifuensis* zone. Takahashi et al. (2009) established conodont biozones in the same section as Yao and Kuwahara (1997): the "Sphaeroides" zone corresponds to the late Olenekian (Spathian), the *P. nakatsugawaensis* zone is late Olenekian (Spathian), and the *H. gifuensis* zone is Anisian (Fig. 18). After their conodont biostratigraphic work, Sakuma et al. (2012) correlated $\delta^{13}C_{org}$ records in the Momotaro–Jinja section with high-resolution isotopic profiles of carbonate carbon ($\delta^{13}C_{carb}$) from shallow-marine carbonate sequences in southern China (e.g., Payne

Fig. 16. Aerial photograph of the Unuma section showing the location of Lower Triassic bedded chert sequence described by Yao and Kuwahara (1997).

et al., 2004) to establish a higher-resolution age model.

The basal 3 m of the section is composed of gray siliceous claystone (Bed groups 2 and 3 of Takahashi et al., 2009: Fig. 18) and red siliceous claystone (Bed group 4), both of which belong to the "Sphaeroides" zone. The middle part of the section (~3 m thick), which belongs to the *P. nakatsugawaensis* zone, consists of red siliceous claystone (Bed group 5), gray siliceous claystone interbedded with chert (Bed groups 6–10, 13), and two black chert beds (Bed groups 11–12). The upper part (~1.5 m thick) contains thick alternating gray chert and siliceous claystone (Bed groups 14–15), and corresponds to the *H. gifuensis* zone (Anisian).

The Momotaro–Jinja section provides valuable insights into the relationship between redox history and radiolarian diversity in the Panthalassa Ocean across the Early–Middle Triassic transition. As discussed at Unuma (STOP 1), the total duration of the Early Triassic oxygen-depleted episode was probably a maximum of 10 million years until recovery in the Anisian (Fig. 11). Takahashi et al. (2009) analyzed organic molecules from siliceous claystones and cherts from the Momotaro–Jinja section to clarify the redox conditions during the Early to Middle Triassic (Fig. 18). Their geochemical analysis revealed low pristane/phytane ratios

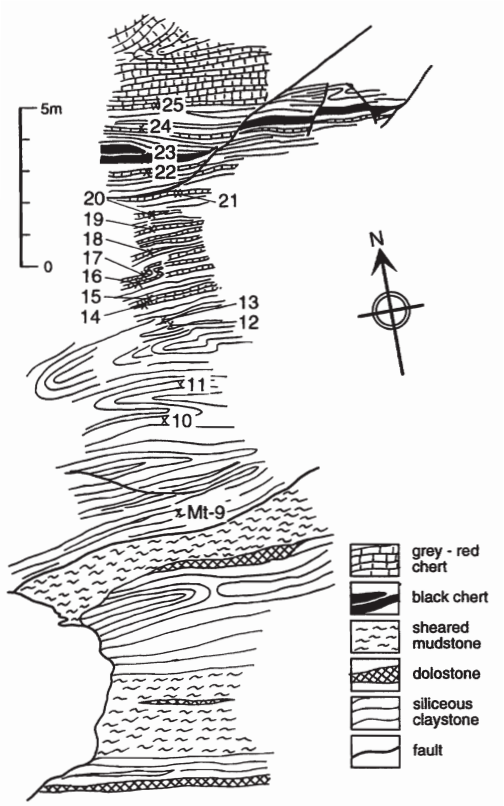

Fig. 17. Sketch of outcrop of the Momotaro-Jinja section at STOP 2-1. After Yao and Kuwahara (1997).

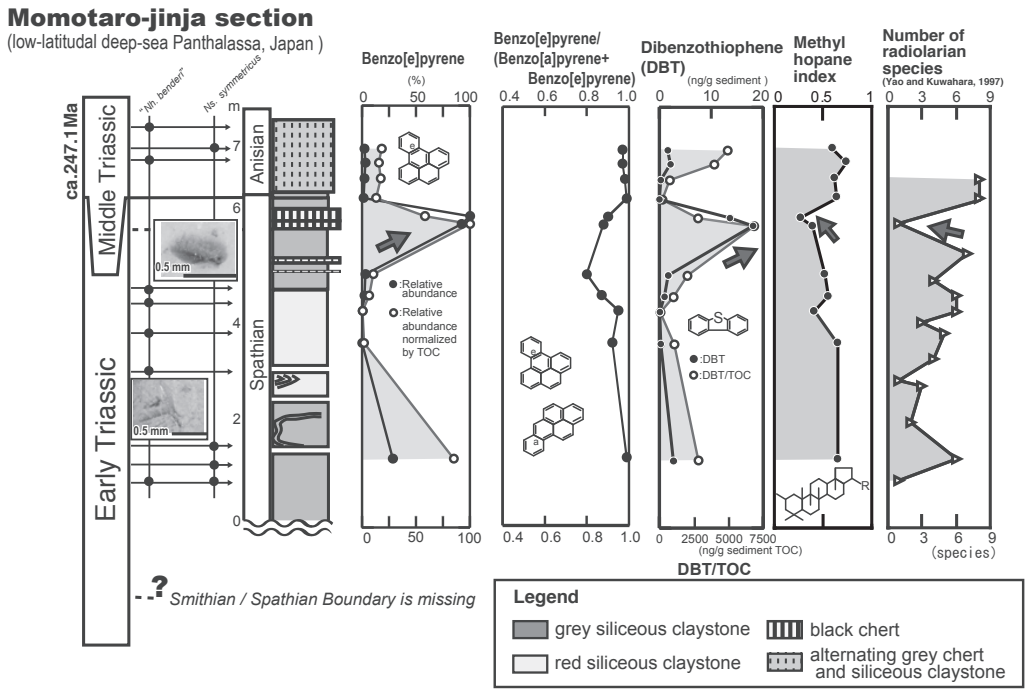

Fig. 18. Study results between Early Triassic and Middle Triassic from the Momotaro-Jinja section of the low latitudinal pelagic deep-sea (after Takahashi, 2013). Data are from Takahashi et al. (2009).

(a measure of redox conditions) in the Momotaro-Jinja section (<1), indicating the prevalence of deep-sea anoxia during the late Olenekian to Anisian. In addition, high concentrations of dibenzothiophene (an index of anoxic depositional environments) are present in the strata deposited at the end of the Spathian, which suggests the development of anoxic deep water. This anoxia event coincided with a decrease in cyanobacterial abundance in the photic zone, as indicated by the 2α-methylhopane index, and low radiolarian diversity. These results suggest that the anoxic deep water in the Panthalassa Ocean reached intermediate water depths at the end of the Early Triassic (Fig. 19), killing marine planktonic organisms including radiolaria (Takahashi et al., 2009).

Stop 2-2: Carnian Pluvial Event

As the stratigraphic sequence youngs from south to north at STOP 2, the Ladinian–Carnian bedded chert sequence was visible in the northern part of the previous stop. The Ladinian and Carnian represent a time of relative stability, interrupted only by an episode of more humid conditions known as the Carnian Pluvial Event (CPE). The CPE occurred in the latest Julian (Early Carnian) and is indicated by several lines of evidence, including a sudden input in coarse siliciclastic material observed in most shallow-water Carnian

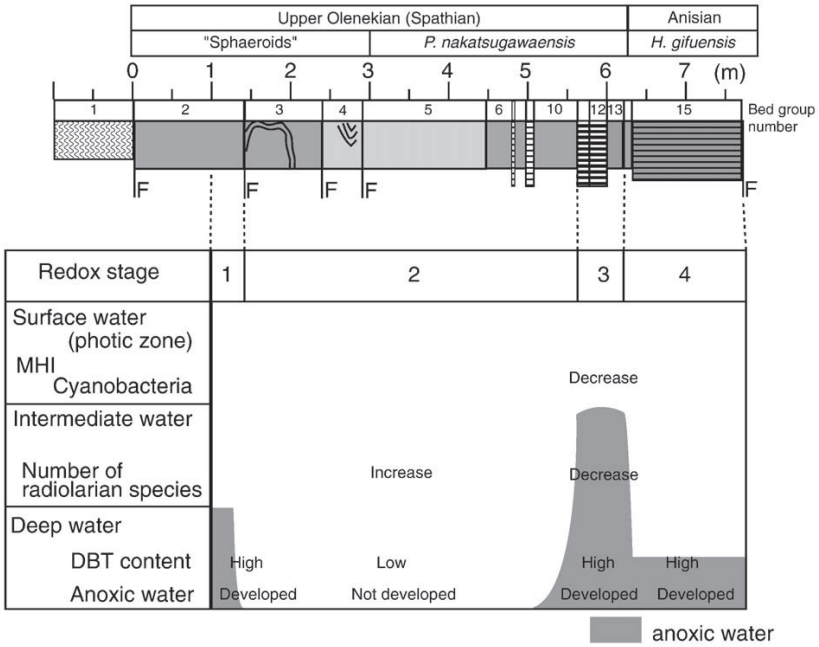

Fig. 19. Conceptual diagram of Panthalassic oceanic environmental stages from the upper Olenekian to lower Anisian. After Takahashi et al. (2009).

successions of Europe (Simms and Ruffell, 1989). The event was characterized by a temporary shutdown of carbonate systems across the western Tethyan realm (Rigo et al., 2007) and high extinction rates of several groups, such as ammonoids, crinoids, bryozoa, and conodonts (Simms and Ruffell, 1989, 1990; Rigo et al., 2007). It has been suggested that the CPE was caused by the major flood-basalt volcanism of the Wrangellia large igneous province in the Panthalassa Ocean (Dal Corso et al., 2012).

To reveal the pelagic sedimentary response to Carnian climate change, Nakada et al. (2014) observed stratigraphic changes in Fe-bearing minerals in the upper Julian–lower Tuvalian interval of the bedded chert sequence from "Section R" (Sugiyama, 1997) at the Momotaro Shrine locality (Fig. 20). They revealed that the stratigraphic change in the Fe-bearing compositions can be divided into three stages: (I) a stage in which a relatively stable mineral composition (chlorite + illite + hematite) is observed in cherts deposited during the lower to middle Julian; (II) an abrupt change in mineral composition (absence of chlorite and appearance of smectite) in upper Julian–lower Tuvalian strata; and (III) recovery of the previous stable mineral composition in the middle to upper Tuvalian (Fig. 21). According to Nakada et al. (2014), the sudden disappearance of chlorite and the presence of smectite during the second stage occurred as a result of increasing rainfall, corresponding to the CPE period. They inferred that the primary formation of chlorite would have decreased, whereas smectite should have formed as a result of the increasing humidity in the continental area.

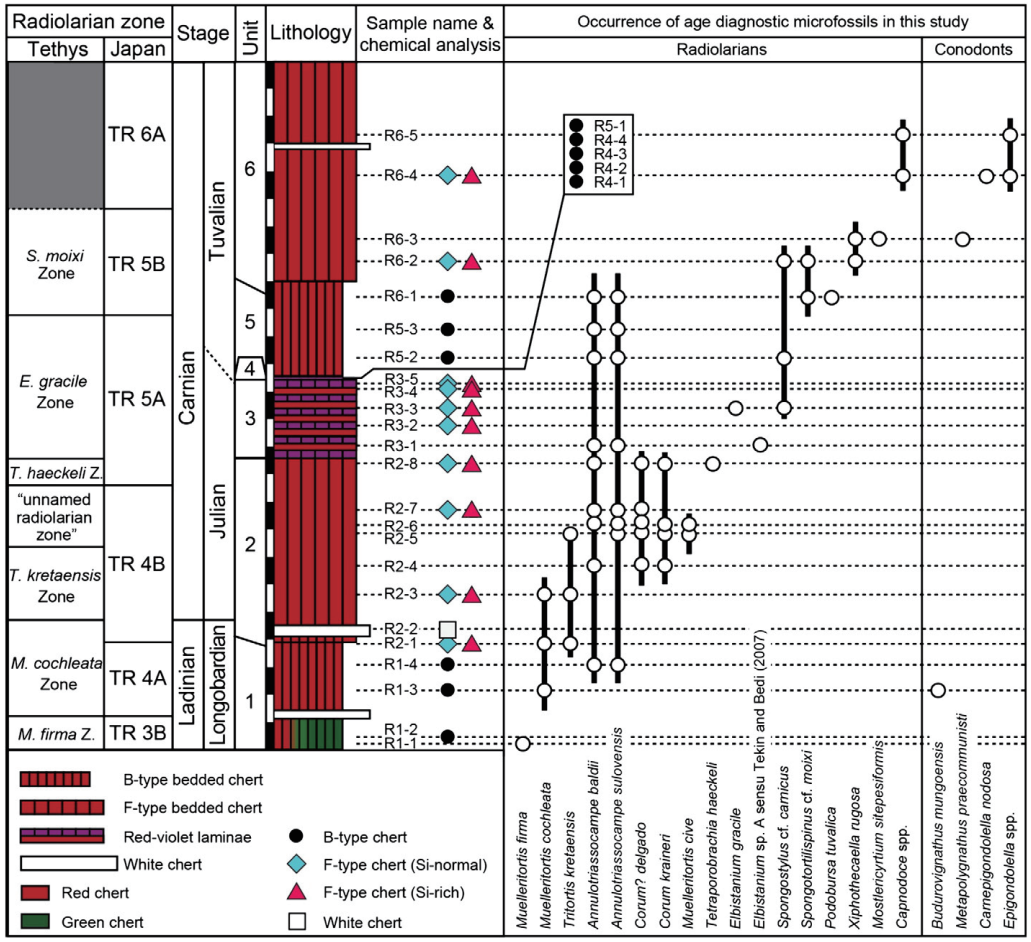

Fig. 20. Summary of lithostratigraphic, biostratigraphic, geochronologic, and examined samples (after Nakada et al., 2014). It is noted that this section is one of the type sections of the Triassic standard radiolarian biostratigraphy by Sugiyama (1997). Radiolarian zones are from Kozur and Mostler (1994) and Kozur (2003) in Tethys and from Sugiyama (1997) in Japan after our examinations of radiolarians and conodonts. The subdivision in the Carnian is based on Ogg (2012). The litholigic types of bedded chert are from Imoto (1984); the B-type bedded chert shows a clear repetition of distinct siliceous and muddy layers at levels of several centimeters and the F-type bedded chert has boundaries that are indistinct due to amalgamation.

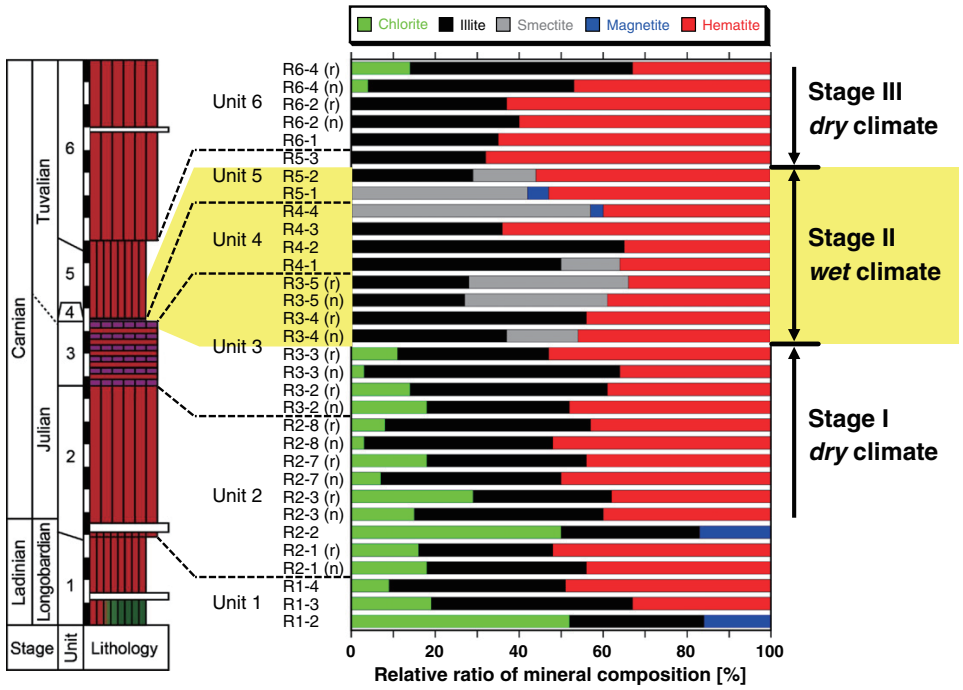

Fig. 21. Summary of XANES- and EXAFS-LCF results for chert samples collected from Section R. The mineral composition determined by EXAFS-LCF prevailed over the XANES-LCF results. Note that (n) and (r) denote the Si-normal and the Si-rich parts of F-type chert, respectively. After Nakada et al. (2014).

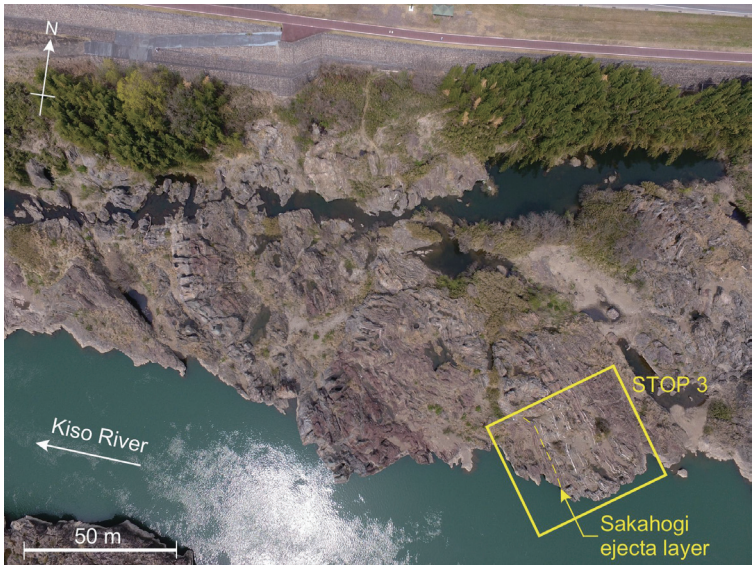

Fig. 22. Aerial photograph of the Sakahogi section showing the location of Norian impact ejecta layer.

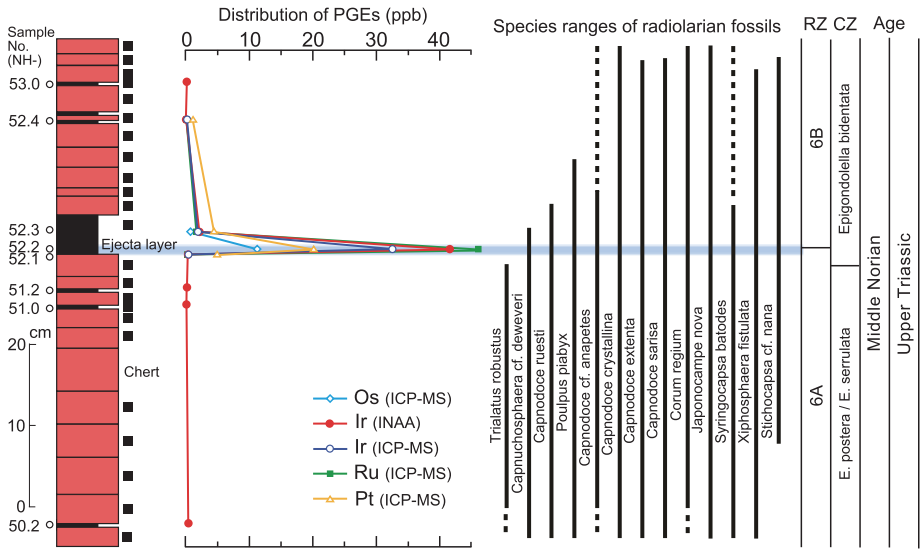

Fig. 23. PGE abundances and biostratigraphy of radiolarians from the middle Norian section (Sakahogi) at STOP 3. Solid squares beside the lithologic section indicate the occurrence of conodonts and radiolarians in cherts and claystones. The radiolarian ranges are used to constrain the age of the ejecta deposit. The claystone contains anomalously high iridium concentrations, of up to 41.5 parts per billion (ppb), which are comparable with the levels found at the K/Pg boundary. Modified after Onoue et al. (2012).

STOP 3. Sakahogi

GPS coordinates: 35° 25'18"N, 136° 58'27"E.

An excellent exposure of Upper Triassic bedded chert (= CH-2 thrust sheet of Yao et al., 1980) is observed in the Sakahogi locality along the Kiso River (Fig. 22). "Section N" (Sugiyama, 1997) exposes a ~20-m-thick sequence of bedded chert. Sugiyama (1997) established six radiolarian zones (the *Capnuchosphaera* to *Praemesosaturnalis multidentatus* zones) from the Carnian–Norian bedded chert in this section.

Stop 3-1: Norian impact event

We will see and discuss a possible link between the late Middle Norian radiolarian extinction and a large impact event. Such an event has been inferred from anomalous concentrations of platinum-group elements (PGEs) and negative osmium (Os) isotope excursions in a claystone layer in an Upper Triassic bedded chert succession in Section N (Figs. 23, 24: Onoue et al., 2012; Sato et al., 2013). The claystone layer is 4–5 cm thick and contains a lower and an upper sublayer (Fig. 25a). The lower sublayer contains microspherules in a matrix of clay minerals (mainly illite), cryptocrystalline quartz, and hematite (Fig. 25b). The upper sublayer is composed of undisturbed clay minerals (illite) and

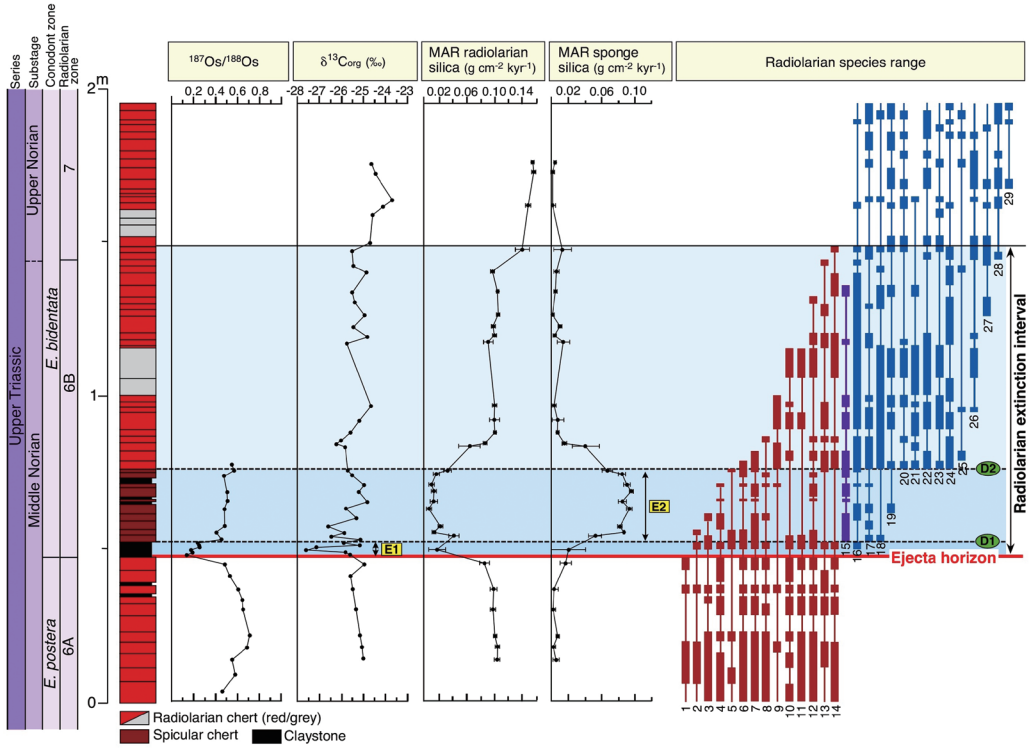

Fig. 24. Stratigraphic profiles of Os isotope ratios, organic carbon isotopes, mass accumulation rates of biogenic silica, and radiolarian biostratigraphy in bedded cherts of the Sakahogi section. Biostratigraphic ranges of 29 radiolarian species in the study interval at Sakahogi show extinctions of middle Norian species (red) corresponding with successive blooms of opportunistic species (purple) and radiations of new species (blue). Dashed lines mark the initial (D1) and second (D2) phases of diversification of upper Norian radiolarian species. Modified after Onoue et al. (2016).

cryptocrystalline quartz.

Biostratigraphic and magnetostratigraphic studies (Sugiyama, 1997; Onoue et al., 2012; Uno et al., 2015) have revealed that the claystone layer occurs in the upper Middle Norian bedded chert. Given that the constant average sedimentation rate of the Middle Norian chert is 1.0 mm kyr^{-1} (Onoue et al., 2012), the deposition of the claystone layer occurred ~1 Myr before the Middle–Late Norian boundary (~214 Ma; Ogg, 2012).

The late Middle Norian age of the clay layer suggests that the PGE anomalies and microspherules in the lower sublayer originated from an extraterrestrial source, related to an impact event that formed the 90-km-diameter Manicouagan crater in Canada (214–215 Ma). In addition, a magnetostratigraphic analysis yielded a normal polarity interpretation for the clay layer, which is consistent with paleomagnetic data for the Manicouagan melt rock (Uno et al., 2015). Studies of PGEs and Os isotopes have revealed that the anomalously high PGE abundances in the lower sublayer resulted from a large chondritic impactor with a diameter of 3.3–7.8 km (Sato et al., 2016). An impactor of this size would produce a crater

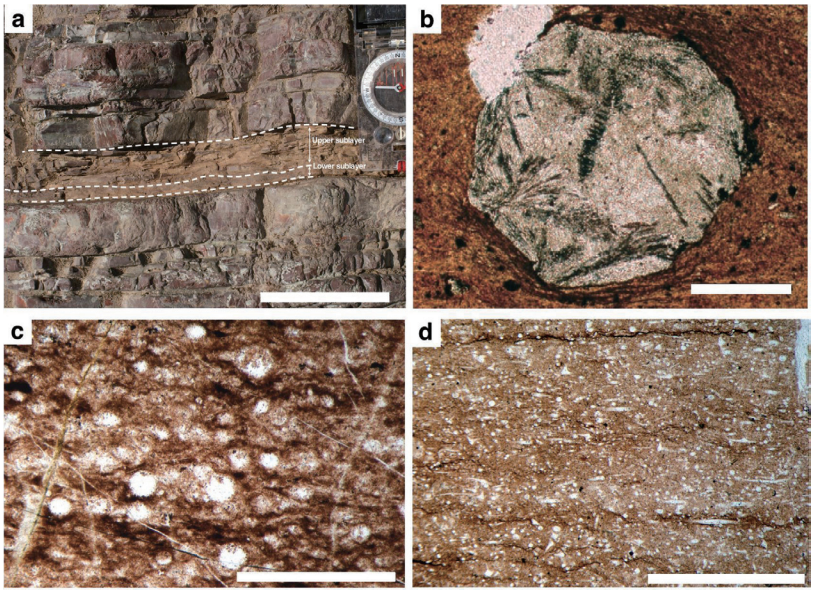

Fig. 25. (a) Photograph showing detail of claystone layer at Sakahogi locality, modified after Onoue et al. (2012). The claystone layer is 4–5 cm thick and contains a lower and an upper sublayer. The lower sublayer contains microspherules in a matrix of clay minerals (mainly illite), cryptocrystalline quartz, and hematite. The upper sublayer is composed of undisturbed clay minerals (illite) and cryptocrystalline quartz. **(b)** Photomicrographs of microspherules from the ejecta deposit. Plane-polarized light. (Scale bar: 500 μm.) **(c, d)** Photomicrographs showing spicular (c) and radiolarian (d) cherts from the Sakahogi section. Plane polarized light. NHR 46 (a); NHR 38 (b). Scale bars = 1 mm.

~56–101 km in diameter, assuming an impactor entry velocity of 20 km s^{-1}, an entry angle of 45°, and a crystalline target (density = 2750 kg m^{-3}). The size range of such a crater is consistent with the size of the Manicouagan crater (diameter = ~90 km).

Stop 3-2: Radiolarian faunal turnover across the Middle–Upper Norian transition

A biostratigraphic study of section N at Sakahogi indicated that extinctions of Middle Norian radiolarian species occurred in a stepwise fashion in the ~1-myr interval above the ejecta horizon (Onoue et al., 2016). Furthermore, high-resolution paleontological and geochemical data (Fig. 24) have revealed that two paleoenvironmental events occurred during the initial phase of the radiolarian extinction interval. The first event (E1) consisted of the post-impact shutdown of primary productivity and a remarkable decline in the amount of biogenic silica preserved before the first phase of diversification (D1). The second event (E2) consisted of a large and sustained reduction in the sinking flux of radiolarian silica and the proliferation of siliceous sponges, which occurred before the second phase of diversification (D2) and lasted for ~0.3 Myr after the impact (Fig. 24). The primary cause of this decline is difficult to identify, but the relatively long period of the E2 interval (~0.3 Myr after the impact) largely excludes the possibility that the decline was triggered by instantaneous environmental stresses (e.g., extended darkness, global cooling, or acid rain)

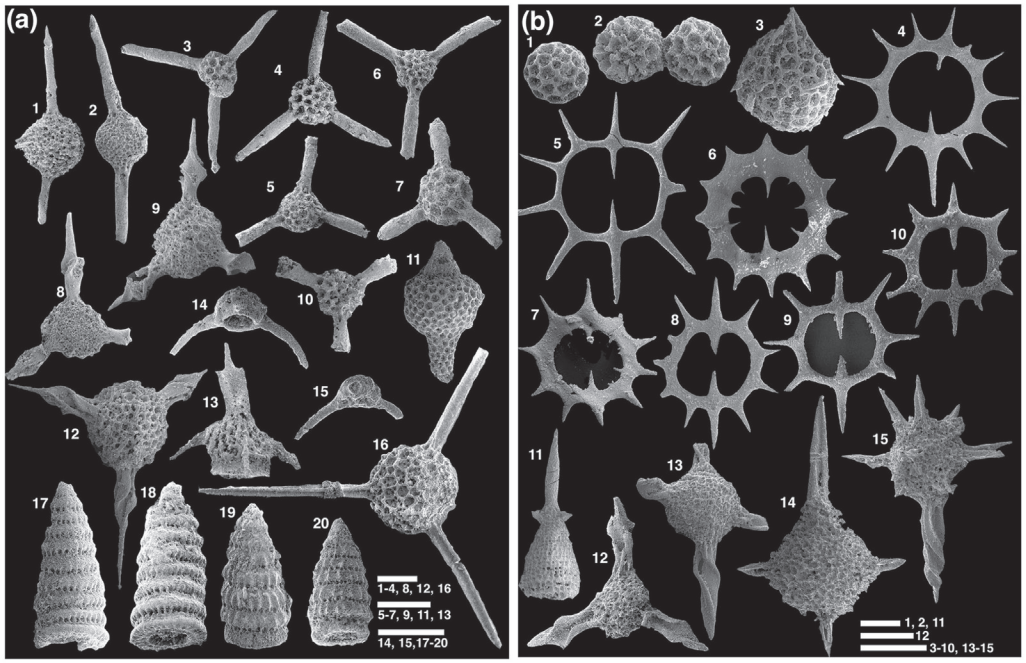

Fig. 26. Radiolarian fossils from the bedded cherts in the middle–upper Norian section at Sakahogi (Modified after Onoue et al., 2016). **(a)** Middle Norian radiolarians from the Sakahogi section. Scale bars = 100 μm. **1–2,** *Xiphosphaera fistulata* Carter. NHR30 (1); NHR49 (2). **3–4,** *Capnodoce sarisa* De Wever. NH52-R6. **5,** *Capnodoce extenta* Blome. NHR50. **6,** *Capnodoce* sp. cf. *C. ruesti* Kozur and Mock. NH52-R6. **7,** *Capnodoce crystallina* Pessagno. NHR43. **8–9,** *Capnuchosphaera* sp. cf. *C. deweveri* Kozur and Mostler. NHR36 (8); NHR53 (9). **10,** *Capnodoce* sp. cf. *C. anapetes* De Wever. NHR31. **11,** *Syringocapsa batodes* De Wever. NH52-R6. **12,** *Sarla hadrecaena* (De Wever). NHR57. **13,** *Trialatus robustus* (Nakaseko and Nishimura). NHR33. **14–15,** *Poulpus piabyx* De Wever. NHR37 (14); NH52-R6 (15). **16,** *Sepsagon longispinosus* (Kozur and Mostler). NHR42. **17–18,** *Japonocampe nova* (Yao). NHR36 (17); NH52-R6 (18). **19–20,** *Corum regium* Blome. NHR43 (19); NH52-R6 (20). **(b)** Upper Norian radiolarians from the Sakahogi section. Scale bars = 100 μm. **1–2,** Spumellaria gen. et sp. indet. A. NHR42. **3,** *Pentactinocarpus sevaticus* Kozur and Mostler. NHR42. **4,** *Palaeosaturnalis harrisonensis* (Blome). NHR52. **5,** *Palaeosaturnalis* sp. aff. *P. dotti* (Blome). NHR81. **6,** *Pseudoheliodiscus heisseli* (Kozur and Mostler) NHR91. **7,** *Pseudoheliodiscus finchi* Pessagno. NHR62. **8,** *Palaeosaturnalis* sp. aff. *P. harrisonensis* (Blome). NHR60. **9,** *Palaeosaturnalis largus* (Blome) NHR57. **10,** *Palaeosaturnalis dotti* (Blome) NHR57. **11,** *Lysemelas olbia* Sugiyama. NHR80. **12,** *Sarla prietoensis* Pessagno. NHR57. **13,** *Plafkerium* sp. A. NHR60. **14,** *Plafkerium* (?) sp. B. NHR74. **15,** *Discofulmen* sp. NHR90.

that would have been caused by a bolide impact.

Decreases in the sinking flux of radiolarian silica during the E1 and E2 events may reflect a decline in radiolarian production in Middle Norian taxa, including in *Capnodoce* and *Capnuchosphaera* species (Fig. 26a). These Middle Norian radiolarians are rare above the E1 interval, whereas a small spumellarian species is abundant within the E2 interval; this spumellarian species is reported as Spumellaria gen. et sp. indet. A, and its occurrence can be used to identify the stratigraphic position of the ejecta layer in other Triassic chert sections within the Jurassic accretionary complexes in Japan (Sato et al., 2013). These taxa can be considered to be short-lived opportunistic species, as they disappeared at the end of

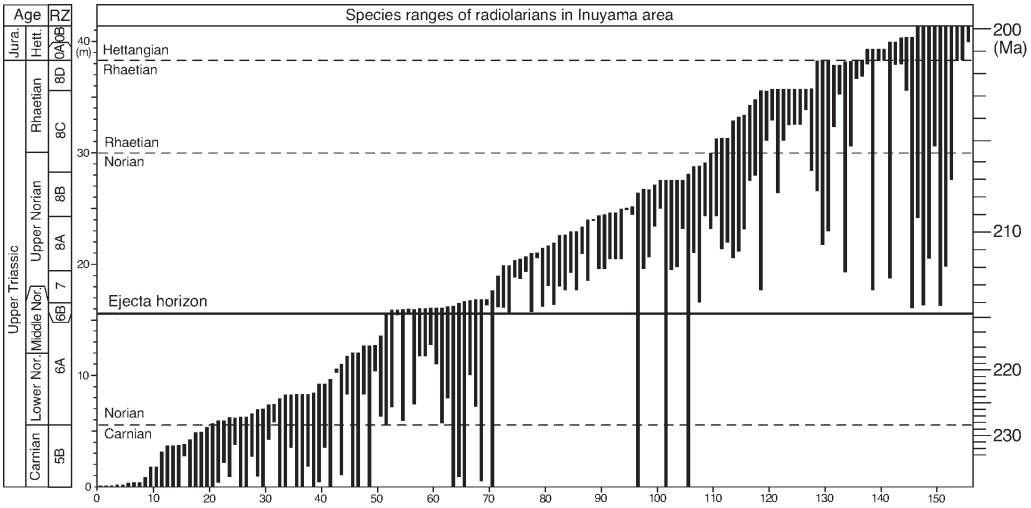

Fig. 27. Stratigraphic ranges of Late Triassic radiolarian species in the Inuyama area, projected onto a composite section, after Onoue et al. (2016). Species numbers are shown on the x-axis. Radiolarian zones (RZ) are from Sugiyama (1997).

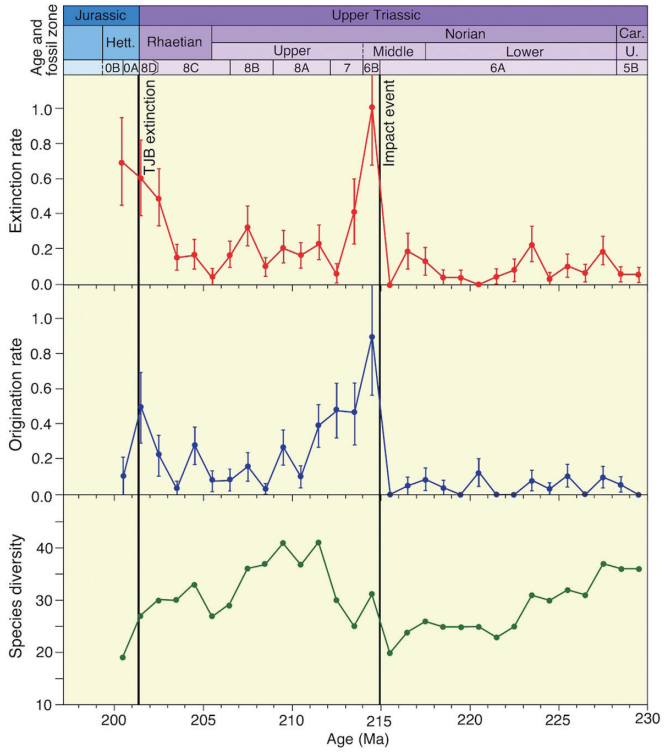

Fig. 28. Extinction and origination rates of Late Triassic radiolarian species in the Panthalassa Ocean. The extinction rate of the middle Norian impact event is substantially higher than the rate at the Triassic–Jurassic boundary (TJB). Error bars are one standard deviation, estimated from bootstrap resampling of the stratigraphic ranges of species with 1000 iterations. After Onoue et al. (2016).

the radiolarian faunal turnover interval. Ito et al. (2017) raised the possibility that these spherical radiolarians represent colonial radiolarians in the Triassic.

The biostratigraphic analysis also revealed that the radiation of Late Norian taxa (Fig. 26b) was contemporaneous with a temporary bloom in the numbers of opportunistic spumellarian species in the E2 interval (Onoue et al., 2016). The timing of these radiation events suggests that the decrease in radiolarian biomass in the Middle Norian taxa enhanced the bloom of opportunistic radiolarian species and the evolutionary radiation of Late Norian taxa in the E1 and E2 intervals. Hence, the gradual extinction of Middle Norian radiolarian taxa during the ~1-Myr period could be explained by ecological pressures imposed by Late Norian taxa, provided that the Late Norian taxa were more rapidly growing and more efficient phytoplankton feeders than the Middle Norian taxa.

Onoue et al. (2016) analyzed a large dataset of Upper Triassic radiolarian occurrences in the Inuyama area to assess the magnitude of the extinction event caused by the Middle Norian impact and to compare this event with extinction events at other stage boundaries (Fig. 27). An analysis of the stratigraphic ranges of radiolarian species indicated that a dramatic increase in extinction and origination rates is observed in the 1-Myr interval following the impact event (Fig. 28). These results suggest that the Middle Norian impact triggered the extinction and contemporaneous evolutionary radiation of the radiolarian fauna in the equatorial Panthalassa Ocean.

STOP 4. Katsuyama

GPS coordinates: 35° 25'21"N, 136° 58'16"E.

A well-exposed outcrop of the bedded chert sequence (CH-3 of Yao et al., 1982) spanning the Middle Triassic to Upper Jurassic, including the Triassic–Jurassic boundary and Toarcian OAE level, is located in the left bank of the Kiso River near Katsuyama, Sakahogi Town, Gifu Prefecture, Japan. This section was originally described by Hori (1990, 1992), and is called the Katsuyama (UF) section. The whole sketch map and stratigraphy of this section were shown in the excursion of Osaka InterRad VII Meeting 1994 (Figs. 29, 30: Matsuoka et al., 1994). Eight radiolarian assemblage zones are recognized: the *Hozmadia gifuensis, Triassocampe coronata,* "*Triassocampe*" *nova, Canoptum triassicum, Parahsuum simplum,* "*Mesosaturnalis*" *(Hexasaturnalis) hexagonus*, and *Parahsuum* (?) *grande* zones.

Stop 4-1: Triassic–Jurassic boundary

The Triassic–Jurassic boundary in the Katsuyama (UF) section is clearly recognized in the CH-3 bedded chert sequence, visible as a color change in the chert facies and an associated thick (<10 cm) shale bed (Hori, 1992). A distinctive dusty red (purplish) chert is developed just above the Upper Triassic brick-red chert sequences, the former is correlated

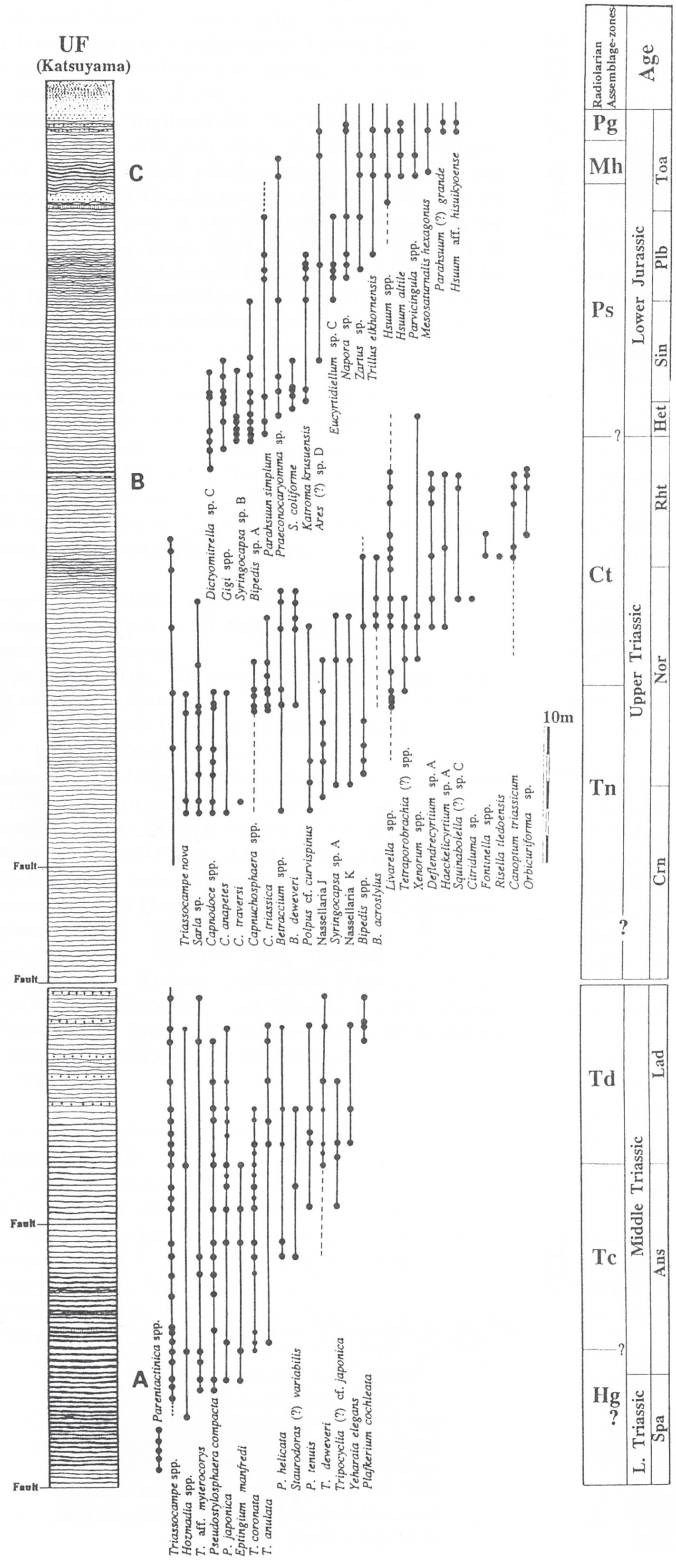

Fig. 29. Lithologic column and stratigraphic distribution of selected radiolarian species in the Katsuyama (UF) section. After Matsuoka et al. (1994).

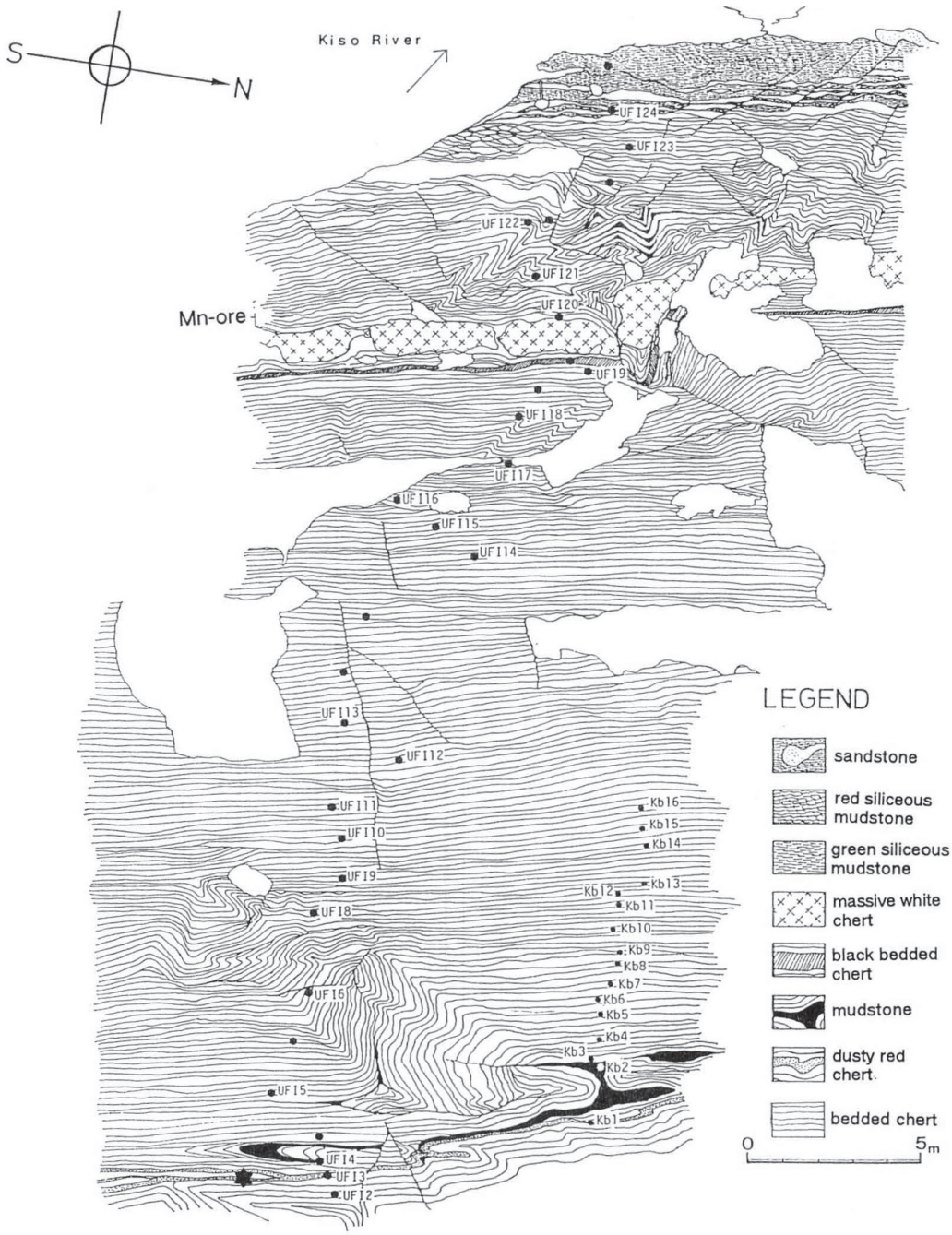

Fig. 30. Sketch map of the Katsuyama (UF) section showing sample localities (solid circles) for radiolarian biostratigraphy of the section. After Hori (1992).

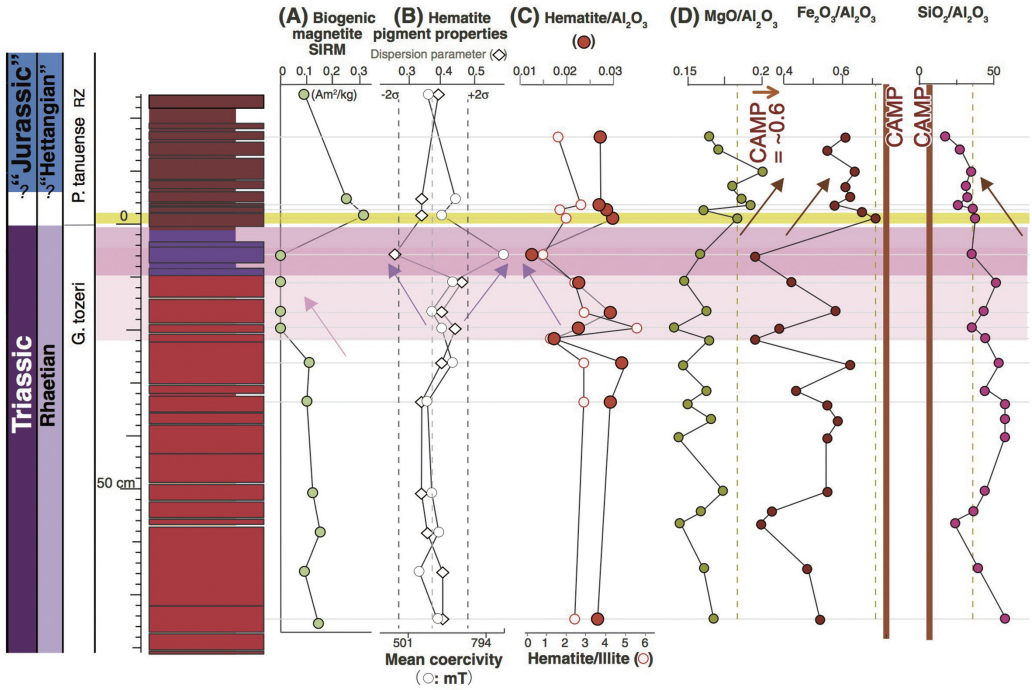

Fig. 31. Stratigraphic changes in magnetic, mineralogical, and geochemical data across the Triassic–Jurassic (T–J) transition at the Katsuyama (UF) section. After Ikeda et al. (2015). (A) Biogenic magnetite saturation isothermal remnant magnetization (SIRM; mA m^2/kg) (Abrajevitch et al., 2013). (B) Hematite pigment properties (Mean coercivity (mT, logarithmic scale; open circle) and Dispersion parameter (DP; diamond)). Dashed red lines indicate range of ± 2 standard deviations from mean for both values (Abrajevitch et al., 2013). (C) Hematite/illite (open circle) and hematite/Al_2O_3 (closed circle) (D) MgO/Al_2O_3, Fe_2O_3/Al_2O_3, and SiO_2/Al_2O_3 ratios. Yellow dotted thin line and brown thick lines indicate the chemical compositions of the base of dusty red chert and the Central Atlantic magmatic province (CAMP) basalts, respectively.

with the final occurrence of the conodont species *Misikella posthernsteini*. The radiolarian faunal change from Triassic to Jurassic taxa occurred after the extinction of *M. posthernsteini* (Carter and Hori, 2005). Distinctive changes in clay and magnetic mineral compositions in the Triassic–Jurassic boundary strata are recognized (Fig. 31), suggesting a short-lived environmental change (pH change?) in the latest Triassic marked by the disappearance of biogenic magnetite (Abrtajevitch et al., 2013) and a reduction in authigenic hematite (Ikeda et al., 2015). The results of Os and C_{org} isotopic analyses on the Triassic–Jurassic boundary chert sequences indicate that similar excursion curves of these isotope ratios have been recognized in Triassic–Jurassic boundary sequences from the Panthalassa such as in New Zealand and the Kurusu section of the Inuyama area (Okada et al., 2015; Hori et al., 2016). These results reveal a long-lived reduction of primary production in the Panthalassa during Late Triassic time and a subsequent increased influx of continental material just before the radiolarian faunal turnover.

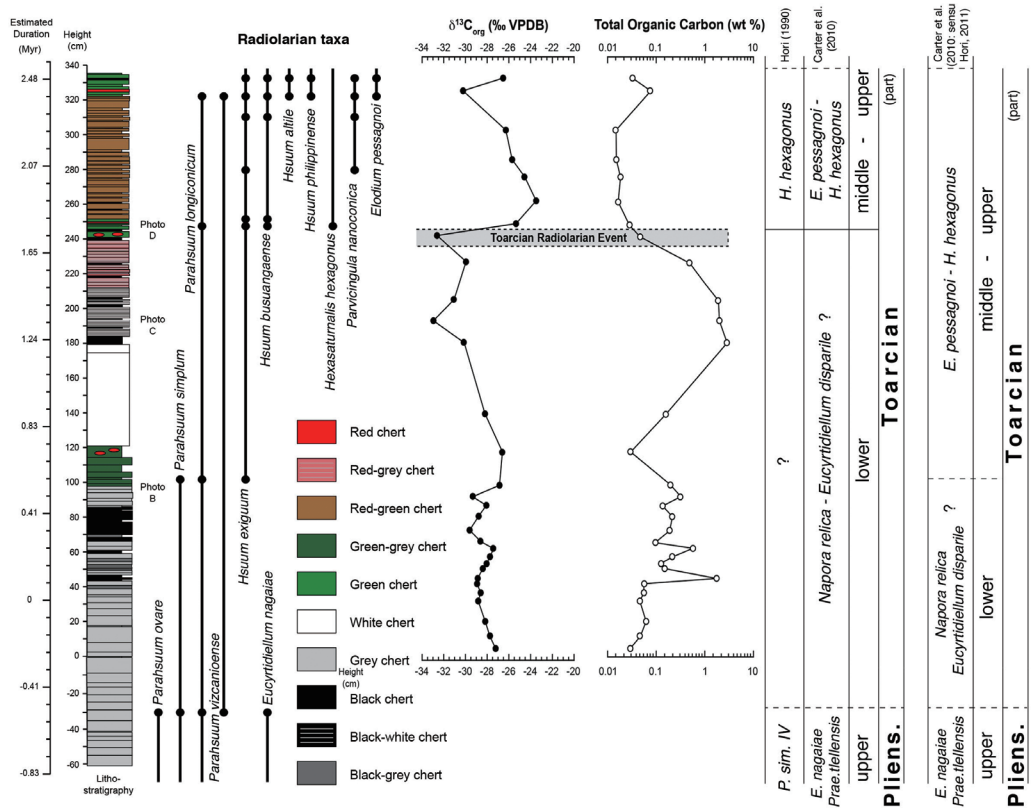

Fig. 32. Detailed lithostratigraphic log, organic carbon isotope record ($\delta^{13}C_{org}$), and biostratigraphy of the Katsuyama (UF) section. Radiolarian biostratigraphy is from Hori (1997) and modified according to Carter et al. (2010). The major difference between these two zonations is based on the presence of only one species (*Hsuum exiguum*) to define to the middle Toarcian. Modified after Gröcke et al. (2011).

Stop 4-2: Toarcian OAE

This section comprises a Toarcian OAE (T-OAE) black chert sequence containing fine, occasionally framboidal, pyrite crystals between the *Parahsuum simplum* and "*Mesosaturnalis*" (*Hexasaturnalis*) *hexagonus* radiolarian zones of the Katsuyama (UF) section. The black chert contains extremely high levels of organic carbon (100 times higher than those of the red cherts from the Inuyama area, which normally contain 0.01–0.03 wt.% organic carbon), with associated overlying thick, massive, white, Mn-rich chert beds. Stable C isotope analysis of organic carbon of bulk cherts yielded a distinctive negative shift at this T-OAE (Fig. 32), indicating an influx of an extremely light carbon source such as methanotrophic bacteria at the time of the T-OAE (Gröcke et al., 2011). A marked radiolarian faunal turnover occurred across this T-OAE level, characterized by disappearance of the *Parahsuum simplum* assemblage radiolarian taxa and a high diversity of multi-segmented nassellarians such as *Hsuum*, *Parahsuum*, *Parvicingula* s.l., and *Elodium* (Hori, 1997). Astronomical cycle analyses of chert bedding revealed that the age and

duration of the T-OAE in the Inuyama chert sequences show good agreement with those of the Karoo–Ferrar volcanism (Ikeda and Hori, 2014).

STOP 5. Kamiaso conglomerate

GPS coordinates: 35° 31'34"N, 137° 6'58"E.

We will observe the Kamiaso conglomerate sandwiched between trench-fill turbidites in the Kamiaso area. The Kamiaso conglomerate is well known because the gneiss clasts within it have yielded the oldest radiometric age in Japan. The conglomerate, together with the sandstone, in the accretionary complex provides important information on the provenance of clastic material (Mizutani, 1959; Adachi, 1973; Suzuki et al., 1991; Takeuchi, 2000). The following descriptions of the geology and chronology of the Kamiaso conglomerate are taken from Adachi (1971), Adachi et al. (1992), and Sano et al. (2013), to which the reader is referred for more detail.

The Kamiaso conglomerate is exposed along the gorge of the Hida River. Four horizons of the conglomerate beds, each several meters thick, have been mapped in this area (Fig. 33), but their lateral extent is limited to less than 1 km. The conglomerate beds, which are intercalated with a mudstone-rich distal turbidite, have sharp bases and are interpreted as channel-fill debris-flow deposits on a submarine fan. Similar conglomerates are known to

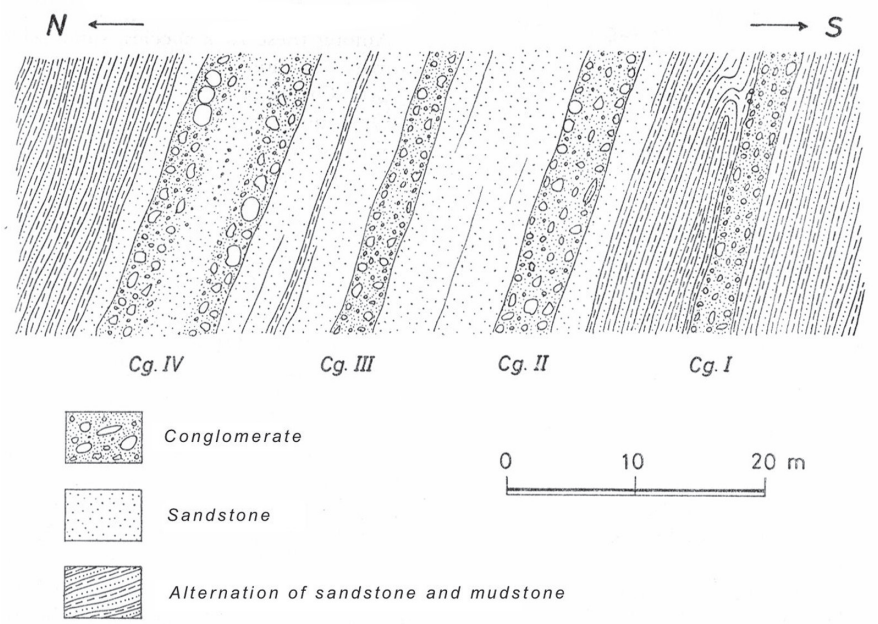

Fig. 33. Kamiaso conglomerate beds intercalated in turbiditic sandstone and mudstone along the Hidagawa River, Kamiaso (after Adachi, 1971).

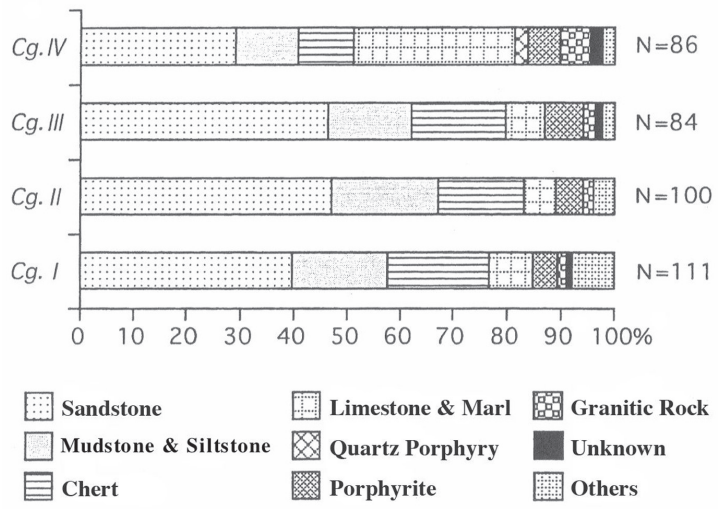

Fig. 34. Clast composition of the Kamiaso conglomerate. Others include orthoquartzite and basalt, and N means the total number of clast samples analyzed (after Sano et al., 2013).

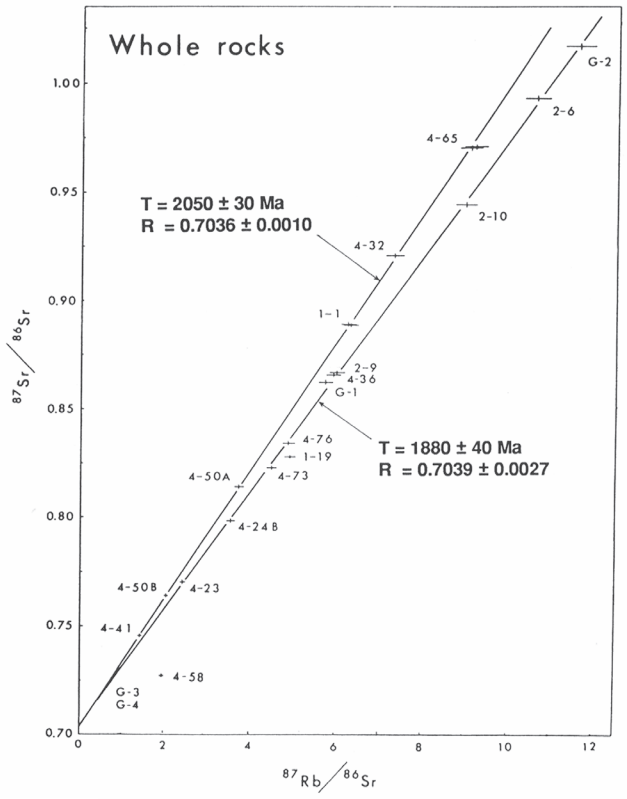

Fig. 35. Rb-Sr whole-rock isochrones for metamorphic and granitic clasts in the Kamiaso conglomerate (after Adachi et al., 1992).

occur at several localities in the Mino Belt. They record episodic events such as mega-earthquakes and mega-storms in the provenance areas, which transported coarse materials to the trench by debris flows.

The conglomerate contains polymictic clasts in a poorly sorted, sandy matrix-supported fabric. The clasts are 1–30 cm diameter, rarely greater than 50 cm. The clast composition is shown in Fig. 34. Intrabasinal rocks such as sandstone, mudstone, siltstone, chert, and limestone are common, and exceptional but key rock species include granitic rocks (including granitic gneiss), orthoquartzite, and marl, which are not components of the Mino accretionary complexes. One of the granitic gneiss clasts yielded a Rb–Sr whole-rock isochron age of 2050 ± 30 Ma (Fig. 35), which is the oldest radiometric age in Japan.

STOP 6. Hisuikyo

GPS coordinates: 35° 32'20"N, 137° 7'34"E.

We will observe the chert sequences at Hisuikyo along the Hida River, where the sequence is similar to that in the Inuyama area. As the Triassic to Jurassic radiolarian and

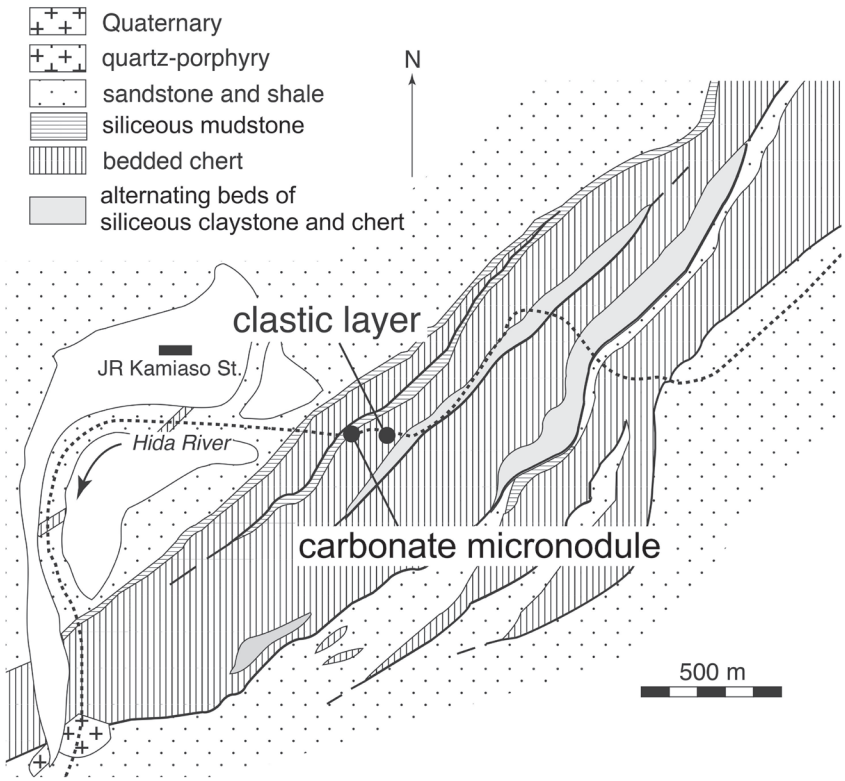

Fig. 36. Geologic map of the Hisuikyo area showing the locations of STOP 6-1 (clastic rock-bearing chert) and STOP 6-2 (manganese carbonate micronodule). Modified from Kido (1982).

conodont biostratigraphies of chert and siliceous mudstone were extensively examined along the Kiso River in the Inuyama area, we will concentrate on the clastic-rock-bearing chert formations and manganese carbonate micronodules at this stop (Fig. 36).

Stop 6-1: Clastic rock-bearing cherts

Chert in the Mino Belt is believed to be pelagic sedimentary rock, given that it lacks coarse clastic material. At some localities, however, the chert beds include clastic fragments such as chert, siliceous mudstone, volcanic rocks (probably basalt), polycrystalline quartz, plagioclase, dolomite, and glauconite (Kojima et al., 1999). In the lower part of the chert section there are 25 chert layers that contain clastic fragments (Fig. 37), although these are actually just 14 layers that have been folded and repeated (Fig. 38). Chert samples (JMP1379, 1380, 1412, and 1413: Fig. 38) yielded radiolarian fossils characteristic of the late Anisian to early Ladinian. The clastic-rock-bearing cherts, however, include both Triassic and Permian

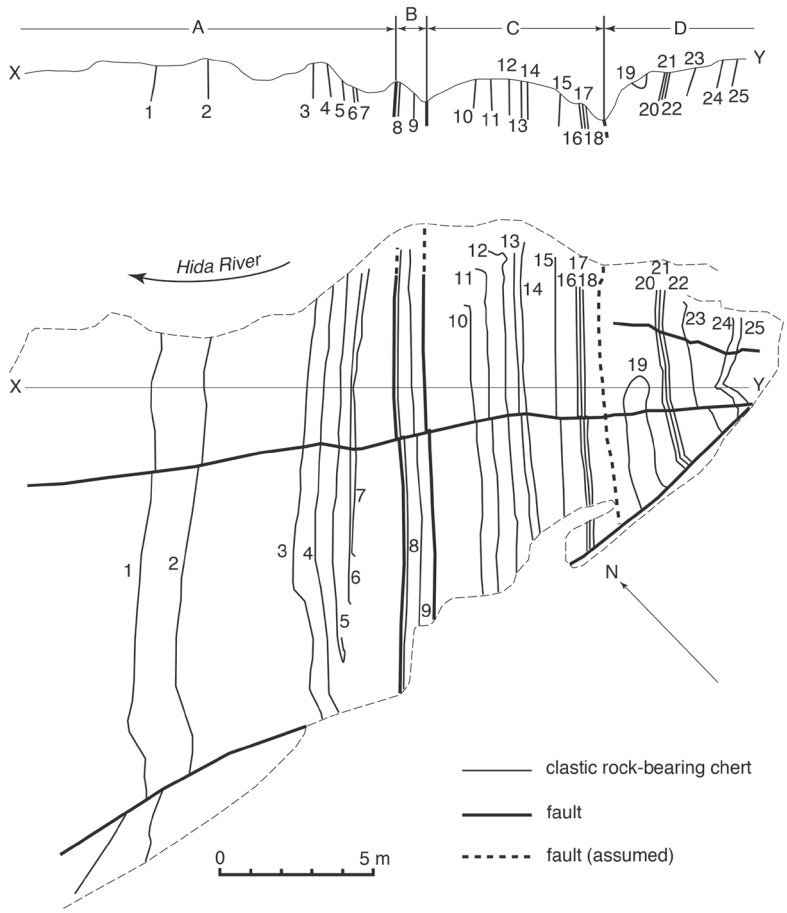

Fig. 37. Map showing occurrence of the clastic rocks-bearing chert in the Hisuikyo area (after Kojima et al., 1999).

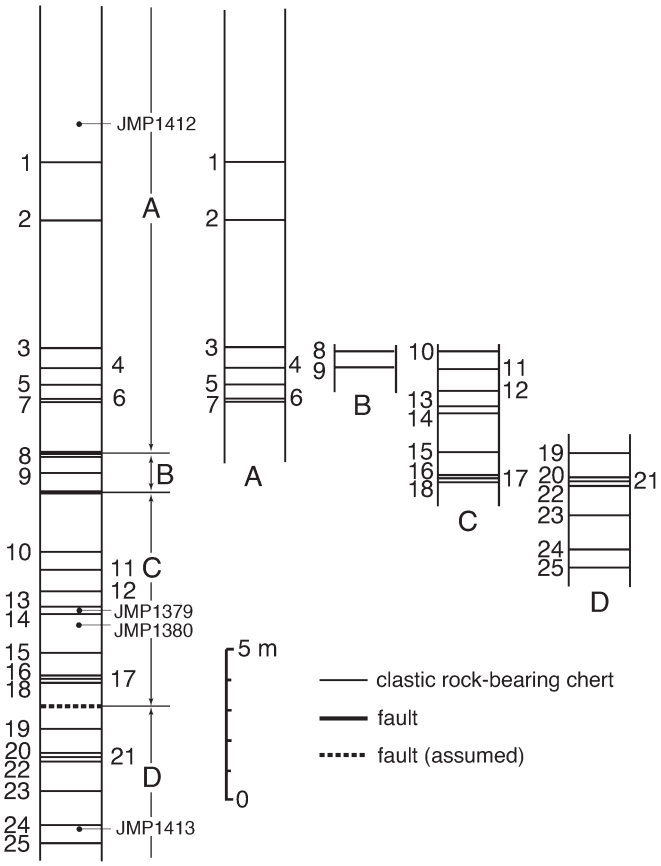

Fig. 38. Columnar sections showing repetition of chert formations in the Hisuikyo area. Left side column shows the apparent succession of the chert, and the other four columns show the correlation of the chert by using the clastic rock-bearing chert, and the numbers with JMP-prefix are horizons of biostratigraphically examined cherts (after Kojima et al., 1999).

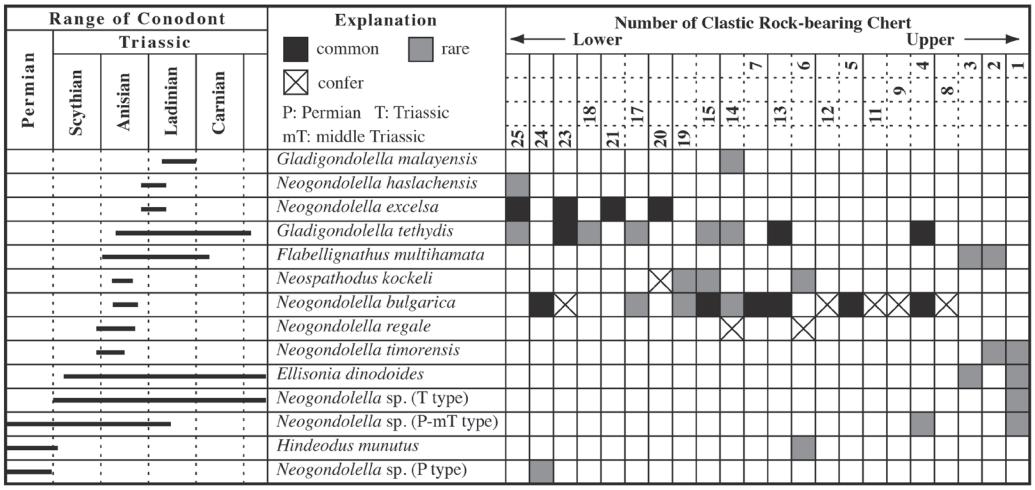

Fig. 39. Occurrence of conodonts from the clastic rocks in chert of the Hisuikyo area (after Kojima et al., 1999).

conodonts (Fig. 39). Although it is difficult to estimate the provenance of the clastic fragments because of their wide variety and small grain size, Kojima et al. (1999) listed volcanic island, island arc, continental shelf, and older accretionary complexes as candidates.

Stop 6-2: Manganese carbonate micronodules

Manganese carbonate micronodules occur in a 10-cm-thick chert formation at the Hisuikyo locality (Figs. 36, 40). The nodules include well-preserved radiolarians, and Isozaki and Matsuda (1985) described new key species from the Early–Middle Jurassic: *Hsuum matsuokai, Laxtorum* (?) *hichisoense*, *Laxtorum* (?) *jurassicum*, and *Transhsuum hisuikyoense*

Fig. 40. Map showing the occurrence of manganese carbonate micronodules in the Hisuikyo section (after Isozaki and Matsuda, 1985).

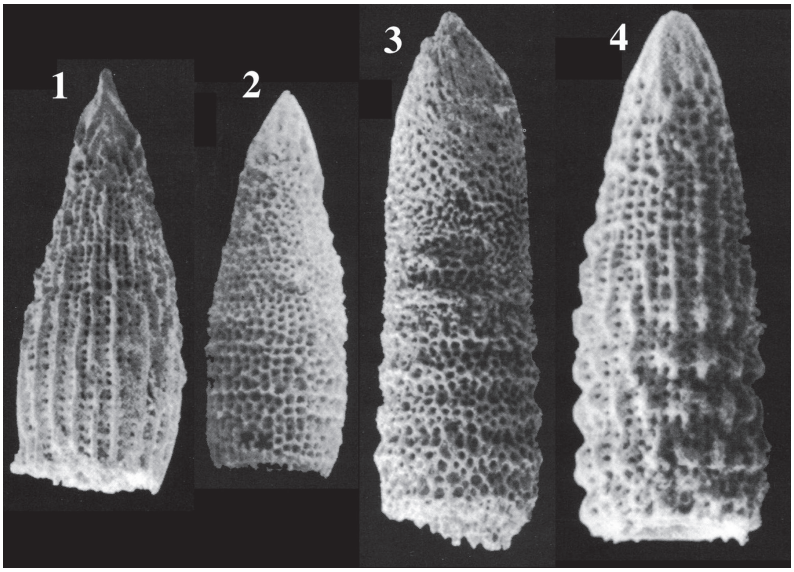

Fig. 41. Radiolarian fossils from the manganese carbonate micronodules in the Hisuikyo section (Reproduced from Isozaki and Matsuda, 1985). **1.** *Hsuum matsuokai*, **2.** *Laxtorum* (?) *hichisoense*, **3.** *Laxtorum* (?) *jurassicum*, **4.** *Transhsuum hisuikyoense*.

(Fig. 41). The micronodule-bearing chert occurs in the upper part of the chert section, and was assigned to the Late Pliensbachian to Bajocian? by Isozaki and Matsuda (1985) and to the Aalenian by Matsuoka (1995). Geochemical studies on the manganese carbonates in the Mino Belt (Sugisaki et al., 1991) suggest a hemipelagic depositional environment. The manganese carbonate nodules and layers always occur near the boundary between the chert and the overlying clastic rocks, and the interpretation by Sugisaki et al. (1991) is consistent with their stratigraphic position.

Concluding remarks

The Triassic–Jurassic chert sequences of the Mino Belt in the Inuyama–Kamiaso area, the Panthalassan pelagic sequences, are one of the most significant and complete records of their ocean environments. Many pioneer works in the 1980s and the early 1990s were shown in the excursion guidebook in previous InterRad held in Japan in 1994 (Matsuoka et al., 1994). Since the publication, further numerous study results have been accumulated, such as Early Triassic ocean anoxia and its recovery (Isozaki, 1997; Takahashi et al., 2009, 2013; Sato et al., 2011, 2012), Late Triassic Pluvial Event (Nakada et al., 2014), Late Triassic bolide impact and radiolarian faunal turnover (Onoue et al., 2012, 2016; Sato et al., 2016), and Triassic–Jurassic astronomical cycles with volcanism (Ikeda et al., 2010, 2015; Ikeda and Hori, 2014; Ikeda and Tada, 2014). We here show these results from the milestones in the

seminal stage to recent achievements on the cutting edge. We hope this excursion guidebook serves as a foundation and will encourage the further development of the studies in the Inuyama–Kamiaso area.

References

Abrajevitch, A., Hori, R. S. and Kodama, K., 2013, Rock magnetic record of the Triassic-Jurassic transition in pelagic bedded chert of the Inuyama section, Japan. *Geology*, **41**, 803–806.

Adachi, M., 1971, Permian intraformational conglomerate at Kamiaso, Gifu Prefecture, central Japan. *Jour. Geol. Soc. Japan*, **77**, 471–482.

Adachi, M., 1973, Pelitic and quartzo-feldspathic gneisses in the Kamiaso conglomerate - A study of Precambrian geology in Japan and East Asia. *Jour. Geol. Soc. Japan*, **79**, 181–203.

Adachi, M., Kojima, S., Wakita, K., Suzuki, K. and Tanaka, T., 1992, Transect of central Japan: from Hida to Shimanto. *29th IGC Field Trip Guide Book*, **1**, 143–178.

Ando, A., Kodama, K. and Kojima, S., 2001, Low-latitude and Southern Hemisphere origin of Anisian (Triassic) bedded chert in the Inuyama area, Mino terrane, central Japan. *Jour. Geophy. Res. Solid Earth*, **106**, 1973–1986.

Carter, E. S. and Hori, R. S., 2005, Global correlation of the radiolarian faunal change across the Triassic-Jurassic boundary. *Canad. Jour. Earth Sci.*, **42**, 777–790.

Carter, E. S., Gorican, S., Guex, J., O'Dogherty, L., De Wever, P., Dumitrica, P., Hori, R. S., Matsuoka, A. and Whalen, P. A., 2010, Global radiolarian zonation for the Pliensbachian, Toarcian and Aalenian. *Palaeogeogr. Palaeoclimat. Palaeoecol.*, **297**, 401–419.

Dal Corso, J., Mietto, P., Newton, R. J., Pancost, R. D., Preto, N., Roghi, G. and Wignall, P. B., 2012, Discovery of a major negative $\delta^{13}C$ spike in the Carnian (Late Triassic) linked to the eruption of Wrangellia flood basalts. *Geology*, **40**, 79–82.

Gröcke, D. R., Hori, R. S., Trabucho-Alexandre, J., Kemp, D. B. and Schwark, L., 2011, An open ocean record of the Toarcian oceanic anoxic event. *Solid Earth*, **2**, 245–257.

Hori, R., 1990, Lower Jurassic radiolarian zones of SW Japan. *Trans. Proc. Paleont. Soc. Japan. N. S.*, no. 159, 562–586.

Hori, R., 1992, Radiolarian biostratigraphy at the Triassic/Jurassic period boundary in bedded cherts from the Inuyama area, central Japan. *Jour. Geosci. Osaka City Univ.*, **35**, 53–65.

Hori, R. S., 1997, The Toarcian radiolarian event in bedded cherts from southwestern Japan. *Mar. Micropaleont.*, **30**, 159–169.

Hori, R. S., Cho, C.-F. and Umeda, H., 1993, Origin of cyclicity in Triassic-Jurassic radiolarian bedded cherts of the Mino accretionary complex from Japan. *Island Arc*, **3**, 170–180.

Hori, R. S., Kuroda, J., Ikehara, M. and Suzuki, K., 2016, Geochemical and Os isotopic studies on the pelagic Triassic-Jurassic mass extinction levels. *Goldschmidt Conference 2016 Yokohama Abstract*, 12i.

Ichikawa, K and Yao, A., 1976, Two new genera of Mesozoic cyrtoid radiolarians from Japan. *Spec. Publ., Progress Micropaleont.*, 110–117.

Igo, H. and Koike, T., 1975, Geological Age of the Kamiaso Conglomerate and New Occurrence of Triassic Conodonts in Mino Mountains. *Jour. Geol. Soc. Japan*, **81**, 197–198.

Ikeda, M., Tada, R. and Sakuma, H., 2010, Astronomical cycle origin of bedded chert: A middle Triassic bedded chert sequence, Inuyama, Japan. *Earth Planet. Sci. Lett.*, **297**, 369–378.

Ikeda, M. and Hori, R. S., 2014, Effects of Karoo–Ferrar volcanism and astronomical cycles on the Toarcian Oceanic Anoxic Events (Early Jurassic). *Palaeogeogr. Palaeoclimat. Palaeoecol.*, **440**, 725–733.

Ikeda, M. and Tada, R., 2014, A 70 million year astronomical time scale for the deep-sea bedded chert sequence (Inuyama, Japan): Implications for Triassic–Jurassic geochronology. *Earth Planet. Sci. Lett.*, **399**, 30–43.

Ikeda, M., Hori, R. S., Okada, Y. and Nakada, R., 2015, Volcanism and deep-ocean acidification across the end-

Triassic extinction event. *Palaeogeogr. Palaeoclimat. Palaeoecol.*, **440**, 725–733.

Imoto, N., 1984, Late Paleozoic and Mesozoic cherts in the Tamba Belt, Southwest Japan. Part 1. *Bull. Kyoto Univ. Educ. Ser. B*, **65**, 15–40.

Isozaki, Y., 1997, Permo-Triassic boundary superanixia and stratified superocean: Records from lost deep-sea. *Science*, **276**, 235–238.

Isozaki, Y., 2014, Memories of pre-Jurassic lost oceans: how to retrieve from extant lands. *Geoscience Canada*, **41**, 283–311.

Isozaki, Y. and Matsuda, T, 1982, Middle and Late Triassic conodonts from bedded chert sequences in the Mino-Tamba Belt, Southwest Japan. Part 1: *Epigondolella*. *Jour. Geosci. Osaka City Univ.*, **25**, 103–136.

Isozaki, Y. and Matsuda, T., 1983, Middle and Late Triassic conodonts from bedded chert sequences in the Mino-Tamba Belt, Southwest Japan. Part 2: *Misikella* and *Parvigondolella*. *Jour. Geosci. Osaka City Univ.*, **26**, 65–86.

Isozaki, Y. and Matsuda, T., 1985, Early Jurassic radiolarians from bedded chert in Kamiaso, Mino Belt, Central Japan. *Earth Sci. (Chikyu Kagaku)*, **39**, 429–442.

Ito, T., Zhang, L., Zhang, M.-H., Feng, Q.-L. and Matsuoka, A., 2017, *Guiuva sashidai* n. gen. n. sp., a probable colonial radiolaria from the Lopingian (Upper Permian) in South China. *Palaeoworld*, in press, http://dx.doi.org/10.1016/j.palwor.2017.04.001.

Kameda, J., Hina, S., Kobayashi, K., Yamaguchi, A., Hamada, Y., Yamamoto, Y., Hamahashi, M. and Kimura, G., 2012, Silica diagenesis and its effect on interplate seismicity in cold subduction zones. *Earth Planet. Sci. Lett.*, **317**, 136–144.

Kimura, K. and Hori, R., 1993, Offscraping Accretion of Jurassic Chert Clastic Complexes in the Mino-Tamba Belt, Central Japan. *Jour. Struct. Geol.*, **15**, 145–161.

Kido, S., Kawaguchi, I., Adachi, M. and Mizutani, S., 1982, On the *Dictyomitrella* (?) *kamoensis–Pantanellium foveatum* Assemblage in the Mino area, central Japan. *News Osaka Micropaleontol. Spec. Vol.*, no, 5, 195–210.

Koike, T., 1979, Biostratigraphy of Triassic conodonts. *Prof. Mosaburo Kanuma Mem. Vol.*, 21–77.

Kojima, S., Ando, H., Kida, M., Mizutani, S., Sakata, Y., Sugiyama, K. and Tsukamoto, H., 1999, Clastic rocks in Triassic bedded chert in the Mino terrane, central Japan: their petrographic properties and radiolarian ages. *Jour. Geol. Soc. Japan*, **105**, 421–434 (in Japanese with English abstract).

Kojima, S., Hayasaka, Y., Hiroi, Y., Matsuoka, A., Sano, H., Sugamori, Y., Suzuki, N., Takemura, S., Tsujimori, T. and Uchino, T., 2016, Pre-Cretaceous accretionary complexes. *In* Moreno, T., Wallis, S., Kojima, T. and Gibbons, W., eds., *The Geology of Japan*. Geological Society, London, 61–100.

Kozur, H., 2003, Integrated ammonoid, conodont and radiolarian zonation of the Triassic and some remarks to Stage/Substage subdivision and the numeric age of the Triassic stages. *Albertiana*, **28**, 57–74.

Kozur, H. and Mostler, H., 1994, Anisian to Middle Carnian radiolarian zonation and descrip- tion of some stratigraphically important radiolarians. *Geol. Paläont Mitt. Innsbruck*, **3**, 39–255.

Kubo, K., Isozaki, Y. and Matsuo, M., 1996, Color of bedded chert and redox condition of depositional environment: 57Fe Mössbauer spectroscopic study on chemical state of iron in Triassic deep-sea pelagic chert. *Jour. Geol. Soc. Japan*, **102**, 40–48 (in Japanese with English abstract).

Matsuda, T. and Isozaki, Y., 1991, Well-documented travel history of Mesozoic pelagic chert in Japan: from remote ocean to subduction zone. *Tectonics*, **10**, 475–499.

Matsuoka, A., 1995, Jurassic and Lower Cretaceous radiolarian zonation in Japan and in the western Pacific. *Island Arc*, **4**, 140–153.

Matsuoka, A., Hori, R., Kuwahara, K., Hiraishi, M., Yao, A. and Ezaki, Y., 1994, Triassic-Jurassic radiolarian-bearing sequences in the Mino terrane, central Japan. *Field trip guide book for the pre-conference excursion of INTERRAD VII, Osaka*, Organizing committee of INTERRAD VII, Osaka, 19–61.

Mizutani, S., 1959, Clastic plagioclase in Permian graywacke from the Mugi area, Gifu Prefecture, central Japan. *Jour. Earth Sci., Nagoya Univ.*, **7**, 108–136.

Mizutani, S. and Kido, S., 1983, Radiolarians in Middle Jurassic siliceous shale from Kamiaso, Gifu Prefecture, central Japan. *Trans. Proc. Palaeont. Soc. Japan, N. S.*, no. 132, 253–262.

Nakada, R., Ogawa, K., Suzuki, N., Takahashi, S. and Takahashi, Y., 2014, Late Triassic compositional changes of aeolian dusts in the pelagic Panthalassa: Response to the continental climatic change. *Palaeogeogr.*

Palaeoclimat. Palaeoecol., **393**, 61–75.

Nakae, S., 2000, Regional correlation of the Jurassic accretionary complex in the Inner Zone of Southwest Japan. *Mem. Geol. Soc. Japan*, no. 55, 73–98 (in Japanese with English abstract).

Nakao, K. and Isozaki, Y., 1994, Recovery history from the P/T boundary deep-sea anoxia recorded in pelagic chert in the Inuyama area, Mino Belt, Southwest Japan. *Jour. Geol. Soc. Japan*, **100**, 505–508.

Nakaseko, K. and Nishimura, A., 1979, Upper Triassic radiolaria from Southwest Japan. *Rep., Coll. Gen. Educ. Osaka Univ.*, **28**, 61–109.

Oda, H. and Suzuki, H., 2000, Paleomagnetism of Triassic and Jurassic red bedded chert of the Inuyama area, central Japan. *Jour. Geophys. Res.*, **105**, 25743–25767.

O'Dogherty, L., Carter, E. S., Gorican, S. and Dumitrica, P., 2010, Triassic radiolarian biostratigraphy. *In* Lucas, S.G., ed., *The Triassic Timescale*. Geol. Soc. London Spec. Publ., 163–200.

Ogg, J. G., 2012, Triassic. In Gradstein, F. M., Ogg, J., Schmitz, M. and Ogg, G., eds., *The Geologic Time Scale*. Elsevier, 681–730.

Okada, Y., Hori, R. S., Ikeda, M. and Ikehara, M., 2015, Geolochemical study of Panthalassa deep-sea sedimentary rocks across the Triassic-Jurassic boundary. *News Osaka Micropaleontol. Spec. Vol.*, no. 15, 219–232 (in Japanese with English abstract).

Onoue, T., Sato, H., Nakamura, T., Noguchi, T., Hidaka, Y., Shirai, N., Ebihara, M., Osawa, T., Hatsukawa, Y., Toh, Y., Koizumi, M., Harada, H., Orchard, M.J. and Nedachi, M., 2012, Deep-sea record of impact apparently unrelated to mass extinction in the Late Triassic. *Proc. Nat. Acad. Sci. U.S.A.*, **109**, 19134–19139.

Onoue, T., Sato, H., Yamashita, D., Ikehara, M., Yasukawa, K., Fujinaga, K., Kato, Y. and Matsuoka, A., 2016, Bolide impact triggered the Late Triassic extinction event in equatorial Panthalassa. *Sci. Rep.*, **6**, doi: ARTN 2960910.1038/srep29609.

Payne, J. L., Lehrmann, D. J., Wei, J., Orchard, M. J., Schrag, D. P. and Knoll, A. H., 2004, Large Perturbations of the Carbon Cycle During Recovery from the End-Permian Extinction. *Science*, **305**, 506–509.

Rigo, M., Preto, N., Roghi, G., Tateo, F. and Mietto, P., 2007, A rise in the Carbonate Compensation Depth of western tethys in the Carnian (Late Triassic): Deep-water evidence for the Carnian pluvial event. *Palaeogeogr. Palaeoclimat. Palaeoecol.*, **246**, 188–205.

Sakuma, H., Tada, R., Ikeda, M., Kashiyama, Y., Ohkouchi, N., Ogawa, N.O., Watanabe, S., Tajika, E. and Yamamoto, S., 2012, High-resolution lithostratigraphy and organic carbon isotope stratigraphy of the Lower Triassic pelagic sequence in central Japan. *Island Arc*, **21**, 79–100.

Sano, H. and Kojima, S., 2000, Carboniferous to Jurassic oceanic rocks of Mino-Tamba-Ashio terrane, southwest Japan. *Mem. Geol. Soc. Japan*, no. 55, 123–144 (in Japanese with English abstract).

Sano, H., Kojima, S., Sato, H. and Rossana, M., 2013, *Guidebook for Field Excursion, Mino belt: Subduction-generated accretionary complex in central Japan, March 17-23, 2013*, Univ. Geneva, 121p., ISBN 978-2-940472-14-7.

Sano, H., Takano, A., Miyamoto, K. and Onoue, T., 2017, Depositional setting of the Upper Triassic siliceous micrite of the Mino-Tamba Belt. *Jour Geol. Soc. Japan*, **123**, 163–178 (in Japanese with English abstract)

Sato, T., Isozaki, Y., Shozugawa, K. and Matsuo, M., 2011, Fe-57 Mössbauer spectroscopic analysis of deep-sea pelagic chert: Effect of secondary alteration with respect to paleo-redox evaluation. *Jour. Asian Earth Sci.*, **42**, 1403–1410.

Sato, T., Isozaki, Y., Shozugawa, K., Seimiya, K., Matsuo, M., 2012, ^{57}Fe Mössbauer analysis of the Upper Triassic-Lower Jurassic deep-sea chert: Paleo-redox history across the Triassic-Jurassic boundary and the Toarcian oceanic anoxic event. *Hyperfine Interact*, **208**, 95–98.

Sato, H., Onoue, T., Nozaki, T. and Suzuki, K., 2013, Osmium isotope evidence for a large Late Triassic impact event. *Nature Commun.*, **4**, 2455, doi: 10.1038/ncomms3455.

Sato, H., Shirai, N., Ebihara, M., Onoue, T. and Kiyokawa, S., 2016, Sedimentary PGE signatures in the Late Triassic ejecta deposits from Japan: implications for the identification of impactor. *Palaeogeogr. Palaeoclimat. Palaeoecol.*, **442**, 36–47

Shibuya, H. and Sasajima, S., 1986, Paleomagnetism of red cherts: A case-study in the Inuyama area, central Japan. *Jour. Geophys. Res.*, **91**, 14105–14116.

Simms, M. J. and Ruffell, A. H., 1989, Synchroneity of climatic change and extinctions in the Late Triassic.

Geology, **17**, 265–268.

Simms, M. J. and Ruffell, A. H., 1990, Climatic and biotic change in the late Triassic. *Jour. Geol. Soc. London*, **147**, 321–327.

Sugisaki, R., Sugitani, K. and Adachi, M., 1991, Manganese carbonate bands as an indicator of hemipelagic sedimentary environments. *Jour. Geol.*, **99**, 23–40.

Sugiyama, K., 1992, Lower and Middle Triassic radiolarians from Mt. Kinkazan, Gifu Prefecture, Central Japan. *Trans. Proc. Palaeont. Soc. Japan, N. S.*, no. 167, 1180–1223.

Sugiyama, K., 1997, Triassic and Lower Jurassic radiolarian biostratigraphy in the siliceous claystone and bedded chert units of the southeastern Mino Terrane, Central Japan. *Bull. Mizunami Fossil Mus.*, no. 24, 79–193.

Suzuki, K., Adachi, M. and Tanaka, T., 1991, Middle Precambrian provenance of Jurassic sandstone in the Mino Terrane, central Japan: Th-U-total Pb evidence from an electron microprobe monazite study. *Sediment. Geol.*, **75**, 141–147.

Takahashi, S., Oba, M., Kaiho, K., Yamakita, S. and Sakata, S., 2009, Panthalassic oceanic anoxia at the end of the Early Triassic: A cause of delay in the recovery of life after the end-Permian mass extinction. *Palaeogeogr. Palaeoclimat. Palaeoecol.*, **274**, 185–195.

Takahashi, S., 2013, Palaeontological and geochemical studies on Permian–Triassic pelagic deep-sea sedimentary rocks. *Res. Org. Geochem.*, **29**, 1–16 (in Japanese with English abstract).

Takeuchi, M., 2000, Origin of Jurassic coarse clastic sediments in the Mino-Tanba Belt. *Mem. Geol. Soc. Japan*, no. 55, 107–121 (in Japanese with English abstract).

Takiguchi, T., Sugitani, K., Yamamoto, K. and Suzuki, K., 2006, Biogeochemical signatures preserved in ancient siliceous sediments; new perspectives to Triassic radiolarian bedded chert compositions. *Geochem. Jour.*, **40**, 33–45.

Tsukamoto, H., 1989, Lutecite in triassic bedded chert from the Southern Terrane, Central Japan. *Jour. Earth Sci. Nagoya Univ.*, **36**, 1–14.

Ujiie, K., Tabata, H., Kinoshita, T., Saito, T., Miyake, A. and Kouketsu, Y., 2015, Linkages between pelagic sedimentation and plate-boundary faulting. *Japan Geoscience Union Meeting 2015 Abstract*, SSS02-06.

Uno, K., Yamashita, D., Onoue, T. and Uehara, D., 2015, Paleomagnetism of Triassic bedded chert from Japan for determining the age of an impact ejecta layer deposited on peri-equatorial latitudes of the paleo-Pacific Ocean: A preliminary analysis. *Phys. Earth Planet. Int.*, **249**, 59–67.

Wakita, K., 1988, Origin of chaotically mixed rock bodies in the Early Jurassic to Early Cretaceous sedimentary complex of the Mino Terrane, central Japan. *Bull. Geol. Surv. Japan*, **39**, 675–757.

Wakita, K., Harayama, S., Kano, K., Mimura, K. and Sakamoto, T., 1992, *Geological map of Japan 1:200,000, Gifu*. Geol. Surv. Japan, 1 sheet.

Yamaguchi, A., Hina, S., Hamada, Y., Kameda, J., Hamahashi, M., Kuwatani, T., Shimizu, M. and Kimura, G., 2016, Source and sink of fluid in pelagic siliceous sediments along a cold subduction plate boundary. *Tectonophysics*, **686**, 146–157.

Yao, A., 1982, Middle Triassic to Early Jurassic radiolarians from the Inuyama area, central Japan. *Jour. Geosci. Osaka City Univ.*, **25**, 53–70.

Yao, A., Matsuda, T. and Isozaki, Y., 1980, Triassic and Jurassic radiolarians from the Inuyama area, central Japan. *Jour. Geosci. Osaka City Univ.*, **23**, 135–154.

Yao, A., Matsuoka, A. and Nakatani, T., 1982, Triassic and Jurassic radiolarian assemblages in Southwest Japan. *News Osaka Micropaleontol. Spec. Vol.*, no. 5, 27–43 (in Japanese with English abstract).

Yao, A. and Kuwahara, K., 1997, Radiolarian faunal change from Late Permian to Middle Triassic times. *News Osaka Micropaleontol. Spec. Vol.*, no. 10, 87–96 (in Japanese with English abstract).

Yoshida, H., 1986, Upper Triassic to Lower Jurassic radiolarian biostratigraphy in Kagamigahara City, Gifu Prefecture, central Japan. *Jour. Earth Sci. Nagoya Univ.*, **34**, 1–21.